Draft version November 25, 2024
Typeset using LaTeX default style in AASTeX631

THUNDER: A Titan orbiter mission concept for the New Frontiers program designed at the JPL Planetary Science Summer School

Cassandra Seltzer,[1] Rudi Lien,[2] Brandon T. Radzom,[3] Ella Mullikin,[4] Kimberly Bott,[5,6] Gwendolyn Brouwer,[7] David G. Burtt,[8] Chloé Gentgen,[9] Jewel Abbate,[10] Victor Gandarillas,[11] Austin P. Green,[12] Tristen Head,[13] Jonathon R. Hill,[14] Jennifer N. Larson,[15,16] Nicholas J. Montiel,[17] M. Regina A. Moreno,[9] Nicholas L. Wagner,[18] Piyumi Wijesekara,[19] James Tuttle Keane,[20] Alfred E. Nash,[20] and Jennifer Scully[20]

[1] *Department of Earth, Atmospheric and Planetary Sciences, Massachusetts Institute of Technology, Cambridge, MA, 02139*
[2] *Department of Earth Sciences, University of Oregon, Eugene, OR, 97403*
[3] *Department of Astronomy, University of Indiana Bloomington, Bloomington, IN, 47405*
[4] *Department of Chemistry, Pennsylvania State University, State College, PA, 16801*
[5] *Department of Earth and Planetary Sciences, University of California Riverside, Riverside, CA, 92521*
[6] *Virtual Planetary Laboratory, SETI Institute, Mountain View, CA, 94043*
[7] *Department of Earth and Planetary Science, University of Hawai'i Mānoa, Honolulu, HI, 96822*
[8] *Solar System Exploration Division, NASA Goddard Space Flight Center, Greenbelt, MD, 20771*
[9] *Department of Aeronautics and Astronautics, Massachusetts Institute of Technology, Cambridge, MA, 02139*
[10] *Department of Earth, Planetary, and Space Sciences, University of California Los Angeles, Los Angeles, CA, 90095*
[11] *Jacobs School of Engineering, University of California San Diego, La Jolla, CA, 92093*
[12] *Planetary Interiors and Geophysics, Jet Propulsion Laboratory, California Institute of Technology, Pasadena, CA, 91109*
[13] *NASA Ames Research Center, Mountain View CA, 94035*
[14] *School of Earth and Space Exploration, Arizona State University, Tempe, AZ, 85287*
[15] *Department of Physics, University of Central Florida, Orlando, FL, 32816*
[16] *SETI Institute, Mountain View, CA, 94043*
[17] *Jackson School of Geosciences, University of Texas Austin, Austin, TX, 78758*
[18] *Department of Geosciences, Baylor University, Waco, TX, 76706*
[19] *Radiation Biophysics Laboratory, NASA Ames Research Center, Mountain View, CA, 94305*
[20] *Jet Propulsion Laboratory, California Institute of Technology, Pasadena, CA, 91109*

ABSTRACT

Saturn's moon Titan is an enigmatic icy world whose surface is constantly modified by its active, Earthlike precipitation system. Here, we propose the THUNDER (Titan's Hydrocarbons: Uncovering New Dimensions of Evolutionary pRocesses) mission concept to investigate how Titan's surface reflects the nature of its interior and its active hydrocarbon cycle. This mission will change our understanding of Titan's surface through three science objectives: characterizing the heat and material transport properties of Titan's icy outer layer, tracing surface liquid storage through and across the crust, and assessing the total hydrocarbon budget through time. This New Frontiers-class mission, designed as part of the Jet Propulsion Laboratory (JPL) Planetary Science Summer School, responds directly to the call for a Titan orbiter in the NASA Planetary Science and Astrobiology Decadal Survey 2023-2032. THUNDER's focused geology and geophysics mission could achieve full surface mapping to complement both the Cassini-Huygens and Dragonfly missions using gravity science, radar with three operational modes, and a visible-to-infrared spectrometer. These instruments together could give us the first look at Titan as a fully connected and geologically active world , revolutionizing our understanding of icy bodies, fluvial and atmospheric processes, and habitability across geologic time. Here, we summarize goals of the science mission and engineering approaches, as well as challenges and future directions to study before THUNDER can become a viable mission concept.

1. INTRODUCTION

1.1. *Why Titan?*

Titan is the only icy ocean world in our Solar System that hosts an active precipitation cycle (Hörst 2017). Complex organic material precipitates from Titan's hazy, nitrogen-rich, Earthlike atmosphere, and has the possibility to develop necessary compounds for biologic activity if it comes into contact with the relatively warm subsurface ocean or interacts with water ice-rich bedrock. This hydrocarbon material moves through Titan's atmosphere before converting to precipitation and haze particles and collecting in lakes and rivers on the surface, and may also travel through the shallow subsurface. To understand Titan's habitability, we must therefore investigate its hydrocarbon cycle.

Titan's surface records its history and development, keeping track of how material may be transported beneath and through Titan's shell. Here, we propose the THUNDER (Titan's Hydrocarbons: Uncovering New Dimensions of Evolutionary pRocesses) mission, which was developed over the course of ten weeks as part of the Jet Propulsion Laboratory (JPL) Planetary Science Summer School (PSSS) in 2023. Using extensive surface mapping, THUNDER will assess the development of Titan into the world we see today, changing our understanding of surface processes across the Solar System, with three scientific objectives:

1. Determine if Titan has a convective ice shell that can facilitate material transport between the surface and ocean.
2. Determine whether Titan's major liquid hydrocarbon bodies are connected and exchanging material with each other through a subsurface reservoir.
3. Determine whether Titan is losing its atmosphere and surface liquids.

Objective 1 studies the thermal state of the shell, which determines the formation and maintenance of topography and controls the flux of carbon-rich material from surface to interior. We will use the principles of tectonostratigraphy to determine the age and cooling rate of the ice shell, and therefore the convective potential to move hydrocarbons between aqueous and icy environments. Objective 2 studies the traces of liquid hydrocarbons as they move between lakes, seas, and the icy subsurface in the outermost parts of Titan's shell. THUNDER will record the signatures of material transport through warm, active regions, as reflected in the surface liquid distribution, budget, and composition. Objective 3 investigates whether Titan's atmosphere is a remnant of past tidal heating which initiated convection in Titan's ice shell and created a massive surface ocean of hydrocarbon liquids released from the interior. This ocean would have permitted the formation and maintenance of an atmosphere with a limited lifespan, such that conditions enabling prebiotic chemistry might disappear within a short geologic time interval. Surface mapping will determine the age of the surface and liquid inventory, and therefore the atmosphere through time.

After addressing these objectives, we will be able to determine how Titan's organic cycle has co-evolved with its interior and atmosphere, and how these processes inform the surface as we see it today. THUNDER will use extensive surface mapping to characterize why Titan is unique among Solar System bodies, and whether its surface characteristics reflect uniquely habitable processes. Establishing the impact of the hydrocarbon cycle on surface development will help us better contextualize other ocean worlds, none of which have evidence of fluvial activity, and clarify why modern Titan hosts a thick atmosphere, while other similarly sized, possibly active bodies like Pluto do not. We can then understand whether Titan represents a unique, temporarily habitable end member, or if it falls within a range of dynamic, potentially life-supporting worlds within our Solar System.

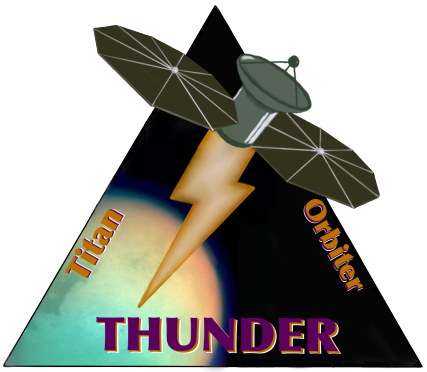

Figure 1. THUNDER mission logo

1.2. *Relevance to NASA programmatic goals and synergy with Dragonfly*

THUNDER directly responds to the call for a Titan mission from New Frontiers 4, and addresses NASA's planetary science goals in the 2023-2032 Planetary Science Decadal Survey (including its direct suggestion for a Titan Orbiter). Titan's s active, hydrocarbon-based precipitation cycle, fluvially dissected landscape, and thick atmosphere make it a perfect natural laboratory to investigate many of NASA's Priority Science Questions (*Origins, Worlds, and Life,* 2023). Through comprehensive surface mapping and full-cycle tracking of Titan's hydrocarbons, THUNDER will advance research on Priority Science Questions 5 (Solid body interiors and surfaces), 6 (Solid body atmospheres and climate evolution), and 10 (Dynamic habitability). This mission looks at how Titan's interior structure is reflected on its surface, how the large lakes and seas interact with each other to modify subsurface chemical environments, and how Titan's standing liquid bodies may have depleted with time to maintain its thick, warm atmosphere.

THUNDER will work in conjunction with the Dragonfly mission to advance NASA's science goals. The Dragonfly mission will revolutionize our understanding of Titan's prebiotic chemistry, in high detail and at local scales; THUNDER will provide global maps and geophysical data to redefine our concept of icy moon interiors, subsurfaces, and tectonic processes. The two missions complement each other, as THUNDER creates global context for Dragonfly's focused, small-scale results. Together, these Titan missions will establish a full picture of the enigmatic moon, maintaining scientific momentum within the community and inspiring sustained public interest.

1.3. *Overview of the Planetary Science Summer School program*

The work presented here was designed as part of a three-month extracurricular educational science mission design program run through the Jet Propulsion Laboratory in Summer of 2023. The Planetary Science Summer School (PSSS) aims to educate early career professionals from diverse scientific and engineering disciplines in principles of competitive mission design, using the New Frontiers program call as a blueprint for mission target and objective selection. Admission to the program was based on a competitive process evaluating the career goals, leadership potential, and unique background and skillset of each early-career applicant. Only two members of the team had previous experience with Titan science before attending PSSS, and many members had educational and work backgrounds in disciplines outside of Solar System planetary science. Several team members were employed as NASA engineers or postdoctoral researchers, and all others others were students or recent graduates in science and engineering; all work was completed outside of the core work of each team member's regular, full-time work.

Titan was selected early in the mission design school by popular vote, based on the qualities described in sections 1.1 and 1.2. During the course of the mission design school, all team members participated in science question design. Team members worked through principles of hypothesis-driven research in order to establish three core scientific objectives, complete with physical parameters and mission requirements, and create a Science Traceability Matrix. The 18-person team then internally selected representatives to serve as a 'hex team' in the roles of Principal Investigator, Systems Engineer, Project Manager, Capture Lead, Proposal Manager, and Cost Lead; all other members of the group chaired a specific subset of design: Propulsion, Attitude and Control, Mission Design & Navigation, Me-

chanical/Configuration, Ground & Data Systems, Flight Software, Thermal, Command & Data Systems, Instruments, Science, Telecommunications, and Power. Each science objective was led by one member of the PSSS team, each of whom additionally held a chair position. One team member also designed a logo (Figure 1) representing the design and goals of the mission.

The program consisted of multiple weekly science and mission planning webinars, a mission architecture study with JPL's Team X in Week 7, meetings with instrumentation and mission design experts at JPL, and an in-person 'Culminating Week,' during which each team member worked with a counterpart on JPL's Team-X to design mission specifics that met the science-driven requirements. On the final day, the hex team presented the THUNDER mission concept to a mock NASA review board, comprised of scientists, engineers, and administrative staff from JPL and NASA Headquarters.

This paper summarizes the scientific objectives and resultant engineering design for the THUNDER mission, much of which was completed in the span of the onsite Culminating Week at JPL. This mission concept is therefore early and necessarily incomplete. We present this work as an educational exercise highlighting the scientific and design work conducted during the three-month course. To this end, we have presented the study close to how it appeared at the conclusion of the course. Given that we are aware that the work may not reflect the best possible approaches, we have also included a section for each science objective describing current challenges, unknowns, and remaining areas for study related to that objective (Sections 2.6, 3.6, 4.5), providing a potential pathway for a dedicated, cohesive mission design in the future. While preliminary, we hope that the science work within this mission concept makes a compelling science case for Titan as a key exploration target in the future of Solar System science.

2. OBJECTIVE 1: DETERMINE IF TITAN HAS A CONVECTIVE ICE SHELL THAT CAN FACILITATE MATERIAL TRANSPORT BETWEEN THE SURFACE AND OCEAN

2.1. *Science rationale*

The thermal state and transport potential of Titan's ice shell constrains the moon's dynamic habitability. The complex organic molecules created in Titan's atmosphere and on its surface include precursors for prebiotic chemistry (He & Smith 2014; Hörst et al. 2012), but Earthlike biological activity cannot develop from these materials unless they are able to access water-rich environments such as Titan's deep ice shell and ocean (Lunine et al. 2020). If the ice shell is convecting, it may be possible that complex organic molecules are advected downwards into the ocean over geological time scales. Similarly, methane and other hydrocarbons degassed during the hydration of the silicate core may be brought up through a convecting ice shell and onto the surface, which could then serve as the source of methane resupply necessary to maintain a stable Titan climate. Furthermore, the nature of the interface between Titan's interior hydrosphere and its silicate core is also a function of the propoerties of the hydrosphere: there is a non-unique solution for Titan's internal structure based on Cassini gravity and topography (Nimmo & Bills 2010; Hemingway et al. 2013; Lefevre et al. 2014; Mitri et al. 2014; Čadek et al. 2021), yielding two possible end members for core-ocean contact. Based on moment-of-inertia calculations, if Titan's ice shell is relatively thin and therefore conductive, the liquid ocean may be directly in contact with the silicate core; if the ice shell is thicker, and therefore convective, there is likely a high-pressure ice layer dividing the ocean from the core, and therefore possibly limiting transport of material outwards (Kalousová & Sotin 2020a). The magnitude of Titan's gravitational response to tides will also change depending on whether its ice shell is thick, weak, and convective or thin, strong, and conductive (Mitri et al. 2014). Thus, determining the heat transport capacity of the crust is essential for untangling the relationship between Titan's tidal evolution and its interior structure. Characterizing the structure, rheology, and tectonism of the ice shell is necessary for determining the dynamic habitability of Titan through time. Figure 2 illustrates these two endmembers: a convective ice shell, seen in Figure 2a, will have a thick crust, covered with contractive features, while a purely conductive ice shell, as in Figure 2b, will be thin and dominated by extensional features.

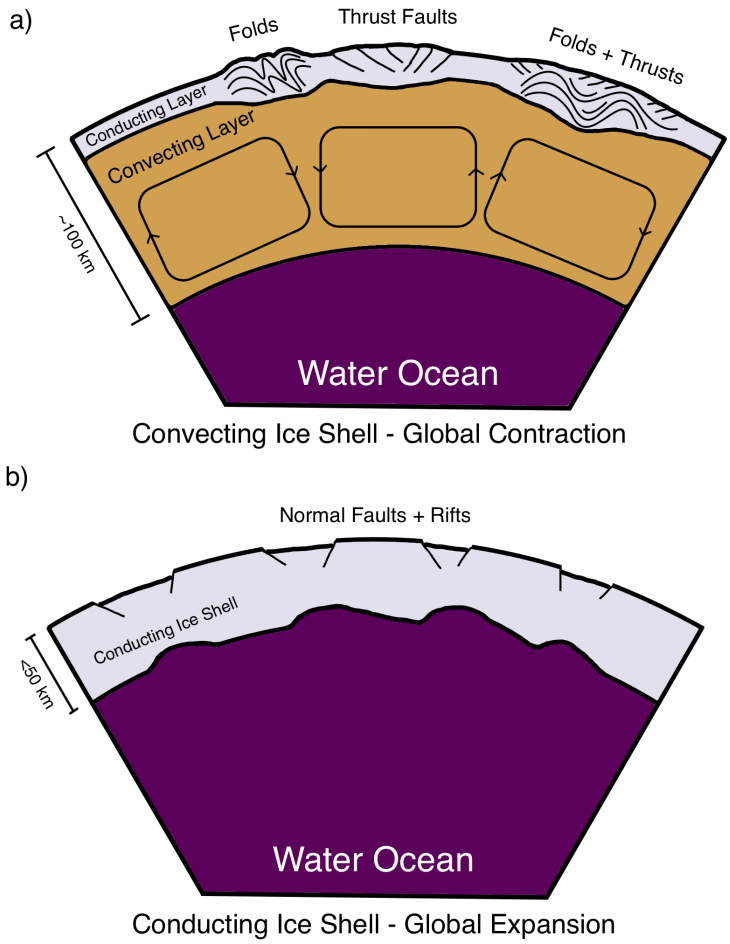

Figure 2. Schematic showing the two endmembers for the state of the Titan's ice shell. a) Convecting ice shell, with a thick convective layer underlying a thin conducting layer. b) Purely conductive ice shell, made up of only a thin conductive layer. Note that only features we aim to test here are present in the graphic; the existence of clathrate layers, finer-scale interior shell structures, and any further solid layers may certainly be present within Titan, but are not depicted.

2.2. *Physical parameter: Admittance*

The thickness and elasticity of the outermost ice layer directly controls the possibility of cryospheric convection. We can therefore use admittance, a transfer function between gravity and topography that is sensitive to the compensation style of the icy outer shell, to measure the convective state of the ice shell. The admittance function represents how much gravity is arising from topography and is sensitive to the compensation style of the cryosphere (Figure 3).

Gravity-topography admittance has been used extensively in the inner solar system on terrestrial bodies to study compensation mechanisms (Wieczorek 2015), and is rigorously defined as the (spherical harmonic) spectral cross power between gravity and topography over the (spherical harmonic) spectral power of topography (Wieczorek 2015) at spherical harmonic degree (n).

As admittance is sensitive to the shape of density contrasts in a planetary interior, we can use it to probe the thermal and viscosity profile of Titan's hydrosphere , where ice may be able to reach isostatic and hydrostatic end-members during a geologically reasonable amount of time (Ermakov et al. 2017; Čadek et al. 2019; Beuthe 2021). The method of admittance has previously been used to demonstrate how varying thermal regimes, influenced by varying tidal heating and the viscosity profile of the ice shell, systematically change the admittance spectrum for Europa and Enceladus (Akiba et al. 2022). Titan's admittance will vary proportionately with the thickness of its ice shell, such that a thicker, convective shell will have higher admittance and a thinner, conductive shell will show lower admittance (Figure 3). THUNDER will significantly improve our coverage of Titan's gravity field (Figure 4), allowing us to study admittance in high detail. As the thickness of the shell directly relates to the heat flux, this technique is justified in order to

175 determine the thermal state of the shell, and definitively say whether the ice shell of Titan is convective or conductive
176 in nature.

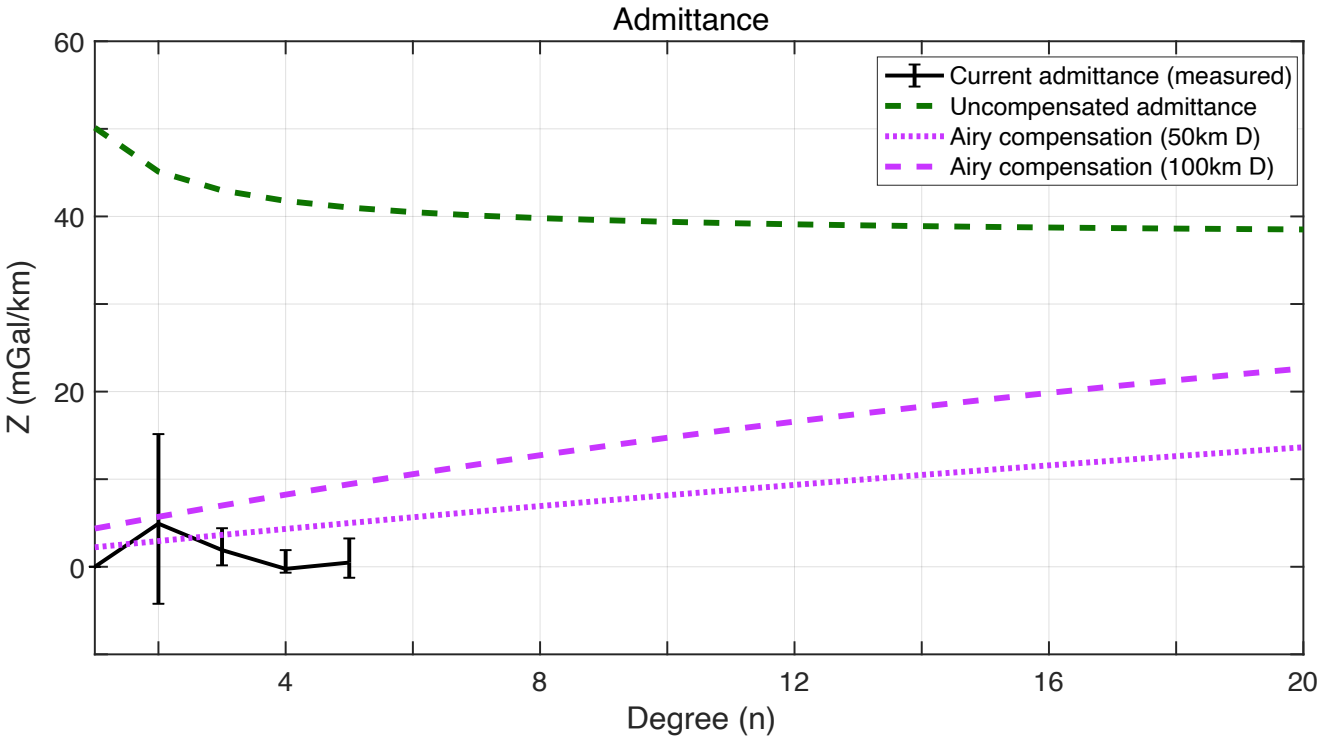

Figure 3. Plotted in black is the current gravity for Titan with associated uncertainties (Durante et al. 2019). We have also plotted theoretical admittance curves for an uncompensated, thin and elastic ice shell, and pure Airy isostatic end-members, indicative of a thicker, viscoelastic shell, with varying ice shell thickness (Akiba et al. 2022).

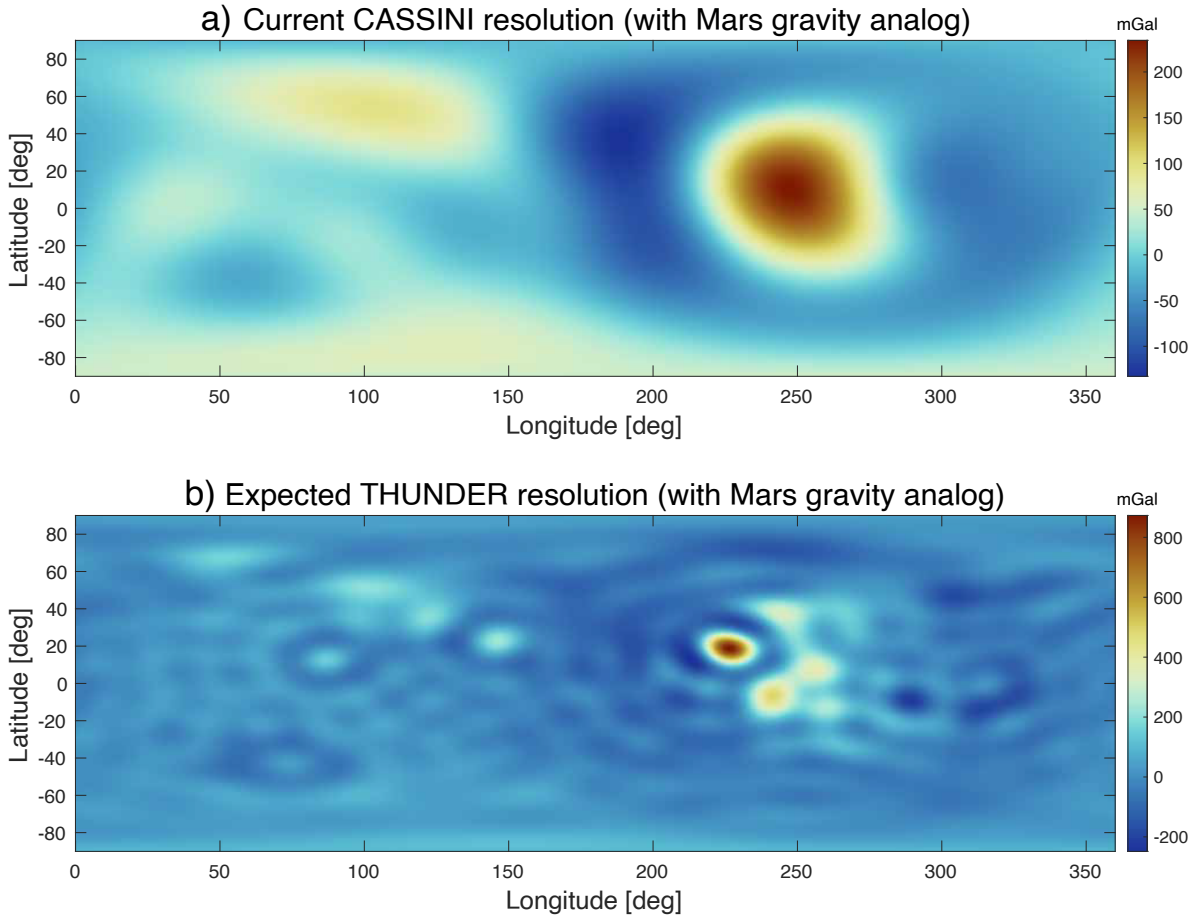

Figure 4. Plotted is an example of our current resolution of gravity data compared with what we would expect THUNDER to resolve. The gravity data plotted is from Mars (Genova et al. 2016) and in subfigure a expanded to spherical harmonic degree 5 (Durante et al. 2019) and in subfigure b expanded to spherical harmonic degree 20. At most, THUNDER is expected to resolve Titan's gravity field up to degree 20.

2.3. *Physical parameter: Tectonostratigraphy*

Generally, icy bodies undergo expansion as their internal heat is lost and their interior oceans solidify (Lorenz 2014a). Titan is unique among icy moons in that current surface mapping is not dominated by the extensional features common on other icy worlds like Enceladus or Europa (Mitri et al. 2014). However, the presence of a thick atmosphere and surface liquids will reduce the scale of topography through erosion, rates of which are poorly constrained on Titan. SAR and altimetry data from Cassini are not sufficient to distinguish between the two end-member thermal cases for Titan's ice shell, as the precise morphology and tectonostratigraphic relationships between contractional and extensional features are essential to understanding its internal structure.

The lack of extensional features may be because Titan's ice shell is in a slow convective state. A convective shell would transport heat from the interior to the surface, inducing freezing that eventually results in a relatively thick crust and high-pressure interior ice phases. As suggested by Mitri et al. (2010), cooling of a convective shell would result in the thickening of a high-pressure ice layer at the base of Titan's interior ocean, ultimately leading to volume contraction. Cooling-induced contraction would then cause young shortening features such as folds and thrust belts, which should be randomly distributed across Titan's surface (Cook-Hallett et al. 2015; Liu et al. 2016). The warmer, convective shell may also be overlaid by a methane clathrate layer, which would encourage convection through thermal insulation and decrease the overall viscosity. If this clathratized shell increases convection, this would suggest that

any long-wavelength topography present on Titan would be dynamically supported. We would therefore expect lower topography, and disagreement with the Airy isostasy model such that ice shell thickness variations (and therefore gravity anomalies, as identified through admittance) are not present in regions of higher topography.

It is also possible that these extensional features do exist, and simply were not resolved by Cassini imaging. If the ice shell is not convecting, it will lose heat through conduction, which is less efficient. A conductive lid will therefore insulate the subsurface ocean while depressing heat flow in the ice shell. This inhibition of heat loss from Titan's interior will limit the growth of high pressure ice phases and result in global expansion (Kalousová & Sotin 2020b). The result of this would be widespread extensional tectonics as seen on other icy worlds in the outer solar system, without recent overprinting by shortening.

The extent of compressive and extensional features across Titan's surface therefore reflects its interior structure and thermal evolution, which in turn inform our understanding of Titan's heat budget and therefore dynamic habitability. We will use photogeologic techniques to map the stratigraphic relationships of different tectonic features on Titan, and to constrain the tectonic mode of its ice shell. Our near-global mapping will allow us to define relative ages of tectonic features via cross-cutting relationships between impact crater populations ('newer' terrain will show fewer craters due to resurfacing) and the development of erosional features. As Titan is a fluvially modified world, we can use fluvial erosion to interpret the recency of landforms. Ancient river networks will reflect the paleotopography at the time of their formation, which may diverge significantly from their current topography depending on the activity of the ice shell in these regions. Larger rivers that have encountered progressively lower grades should show increasing sediment deposition, and any concentration of ancient streams emanating from currently flat regions may indicate that these are former topographic highs, depending on the timescales of relaxation inferred from the thickness of the ice shell.

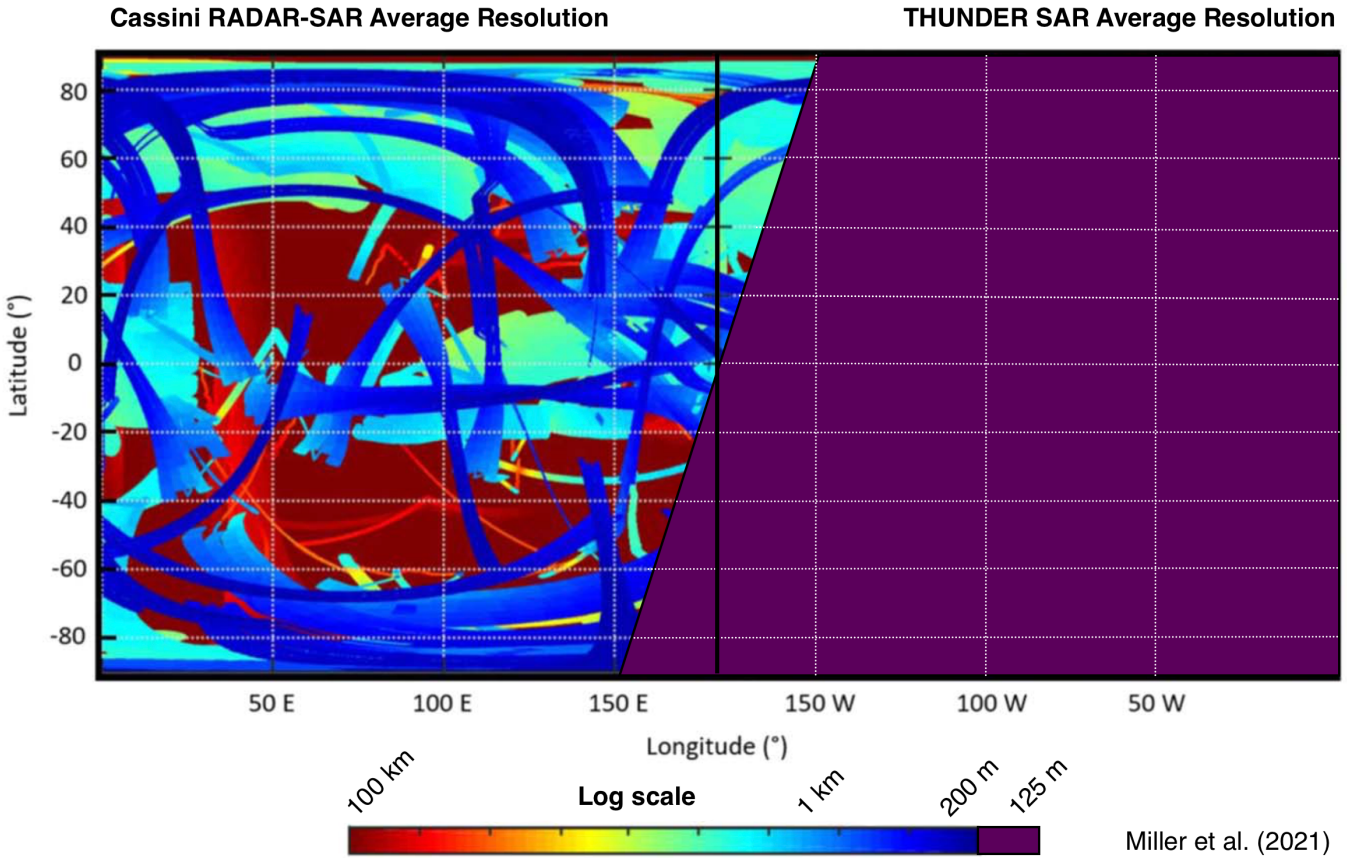

Figure 5. Comparison of the SAR resolution achieved by Cassini RADAR over a subset of Titan's surface (left) and the SAR resolution THUNDER will achieve (right). Figure modified from Miller et al. (2021), where full Cassini resolution is mapped over entire globe. THUNDER will achieve a $\leq$ 125 m/px resolution over the entire surface.

2.4. *Physical parameter: k_2*

The dimensionless complex coefficient k_2 represents how the gravity field of Titan, at spherical harmonic degree 2, is modulated by the tidal effect of Saturn caused by Titan's eccentric orbit. The real part, Re(k_2), quantifies the magnitude change of the gravity field whereas the imaginary part, Im(k_2), quantifies the time lag of this change after it is applied. The thickness of the outer icy shell is directly tied to the value of k_2, as a thinner shell leads to systematically higher values of the real part of this Love number, all else held equal. Conversely, a thicker shell leads to lower values of the real part of k_2. Mitri et al. (2014) have additionally shown that higher values of ocean density lead to higher values of k_2.

Currently, there are discrepant measurements of k_2: a high value of 0.616 ± 0.067 (Durante et al. 2019) and a low value of 0.375 ±0.06 (Goossens et al. 2024). This large uncertainty makes it difficult to use gravity to understand the conditions of the outer icy shell. A lower estimate of k_2 suggests lower values of the thickness of the outer icy shell, whereas a high estimate suggests a low-density ocean with a high thickness. By nature of THUNDER being an orbiter, we will recover k_2 to at least an accuracy of ±0.01, but a thorough trajectory analysis must be conducted to determine this level of accuracy further. To achieve this precision, THUNDER's telecommunications system is equipped with Ka- and X-band up and downlink which allows for high-resolution radio tracking measurements.

THUNDER only requires the real portion of this coefficient in order to meet our science objective, however, a constraint on the imaginary portion of k_2 will additionally be measured. Currently, the uncertainty in this value is larger than the estimate of the value itself (Durante et al. 2019). Thus, any constraint on the imaginary part of k_2 will help constrain the dissipative properties of both outer icy shell and the deep interior, better elucidating Titan's thermal and orbital history.

2.5. *Measurement requirements*

For admittance and (Re(k_2)), a radio tracking precision of 0.01mm/s is needed (a common upper limit for radio tracking with a quasi polar orbit, with parallels from Mars gravity tracking on MRO and plans for Europa orbiter; Konopliv et al. 2011; Blanc et al. 2020). This will allow THUNDER to achieve the necessary measurement at the required level to answer Objective 1. This precision is achievable with THUNDER's telecommunications system (see Section 7.9). For Physical Parameter 1, topography must be globally acquired through altimetry at a resolution of $\leq$ 1000 km, which can be achieved during initial orbital insertion but will be fully met with the resolution necessary to achieve all other radar requirements. Gravity science measurements related to physical parameter 3 must be taken with 7.5-day spacing between Titan's apoapsis and periapsis.

The necessary resolution for tectonostratigraphy is 125 m/pixel in SAR. This resolution will allow us to resolve small dendritic networks, fault contacts and scarps on the scale predicted for global contraction due to convection, and disentangle the overprinting of these features. Many reported river widths from Cassini SAR are on the order of $\simeq$ 0.5 - 1 km (Burr et al. 2013b); a resolution of 125 m/pixel is therefore sufficient for confirming Cassini data and determining whether the reported range is true, or simply limited by Cassini SAR resolution. Furthermore, this will allow for increased capacity to spot small craters (<0.5 km diameter), which will be crucial for understanding relative surface ages of tectonic features. The necessary altimeter resolution is 30 m vertically (and 500 m/pixel horizontally) in order to both identify different kinds of geological features (including mountains and plains) and create a coarse digital topographic model which, in conjunction with higher-resolution SAR images, can determine the heights of fault scarps, folds, and degree of weathering. SAR and altimetry are required over 78% of Titan's surface (Figure 9), with attention paid to the lakes and mare regions, Xanadu Regio, and hummocky and mountainous terrain across the globe. The lakes and mare regions (>60°latitude N and S) will show drainage networks and fluvial activity, past and/or present, that can be compared to other features across the globe. Detailed coverage will allow us to establish how fluvial networks crosscut each other in relatively flat territory, which will be useful for identifying tectonostratigraphic relationships in higher-topography regions. Xanadu Regio, at roughly 15°S and 100°W, is a unique and anomalous geological unit identified by Cassini and has been tentatively identified as highly tectonized, with extensive but small-scale (> km scale) deformation that resists unambiguous interpretation (Radebaugh et al. 2011). The relative age and style of deformation here would place a key constraint on the convective history of Titan. If the dominant deformation mechanism of Xanadu appears to be contractional, the age of this unit indicates that convection was active during its formation. The hummocky and mountainous terrain crossing the mid-latitutes are also crucial for this study. These geomorphological units preserve medium-scale topography (on the order of 1 - 10s of km horizontally; Lopes et al. 2019a), and therefore sample a wide range of time during which deformation was occurring.

Similar to Xanadu Regio, contraction implies an extreme rate of cooling associated with convection, while extension implies a more stagnant ice shell. However, these regions exhibit a different deformation wavelength and therefore represent a different time period and process than Xanadu. We can establish further comparison between Cassini and THUNDER by imaging Adiri Regio, around 10°S, 210°W. Adiri is an equatorial mountain belt surrounded by dune seas and containing the Huygens landing site. Huygens showed that drainage networks cross this mountainous province (Soderblom et al. 2007), providing an opportunity to analyze the stratigraphic relationships between tectonic episodes.

2.6. *Some challenges and future areas for study for Objective 1*

The planned investigation associated with this science objective is highly complicated by our uncertain understanding of Titan's crustal composition. Without these constraints, our gravitational and tectonic observations will not yield unique solutions. For example, it is highly likely that Titan's crust contains hydrocarbon clathrates, which would provide an insulating effect that controls the degree of outwards heat transport (Kalousová & Sotin 2020b; Carnahan et al. 2022). This clathrate layer could be stable to 5 km or above (Choukroun et al. 2010; Schurmeier et al. 2024). If Titan's shallow subsurface is heavily clathratized, its thermal structure will be significantly warmer than if it is solid ice, leading to a thin, conductive lid that limits the total heat removed through convection (Kalousová & Sotin 2020b). Clathrates would also enhance relaxation of crustal features (although would likely not remove signatures entirely; Schurmeier et al. 2024), adding complexity to the interpretation of feature longevity in regions of thinner or thicker crust. The discussion of crustal parameters in section 2.3 is therefore highly limited. A much more detailed observation of Titan's crust and its thermal structure is necessary in order to answer the questions put forth in this objective as currently written. Radiometric observations directly after rainfall events could provide the necessary thermal changes for observation, but these would require inversion based on the thermal conductivity of any sediment (which is thought to be low;Schurmeier & Dombard 2018) and results from complementary experiments on the radiometric signatures of evaporative cooling from Titan's icy crust. In situ geophysical observations through the passive seismometer on Dragonfly could help constrain the depth of a clathrate lid (Marusiak et al. 2022), in conjunction with the radiometric observations from THUNDER, but further modeling is needed.

Clathratization affects the entire depth of the ice shell, not just the shallow subsurface, and its thermal effects place strong controls on the size and temperature of the subsurface ocean (Carnahan et al. 2022). It is possible that our gravity inversions, if coupled with complementary thermal data, could help to assess the depth of this ocean, and thus provide evidence for the extent of subsurface clathratization. However, the composition of this subsurface ocean, which will further affect inversions of gravity data, is also currently unknown. Magnetometry, instrumentation for which is not included in the current THUNDER design, could be a key tool for interpreting the size and composition of Titan's ocean, as has been proposed for moons in the Jovian system (Biersteker et al. 2023; Petricca et al. 2023). This approach is complicated by the fact that the exploration of Jupiter's moons is aided by the misalignment between the planet's rotation axis and magnetic dipole, while Cassini data showed that Saturn's magnetic field is nearly parallel to its rotation axis (Cassini magnetometer team 2017). The magnetic perturbations of Titan's atmosphere would also strongly affect readings aboard an orbiter, so further study and modeling would be necessary to evaluate its utility at Titan.

Furthermore, it is not possible to conduct the proposed tectonostratigraphic study (Section 2.3) without a stronger understanding of Titan's erosive processes. We do not yet understand the dominant mechanisms of erosion, whether chemical (Neish et al. 2015, 2016) or mechanical (Seltzer & Perron 2023), all of which depend heavily on the unknown composition of the crust; without constraints on dominant erosive mechanisms, timescales of erosion are very difficult to constrain. THUNDER's proposed higher-resolution imaging would yield better insight into the extent of erosional features, but this objective offers no specific hypotheses or experiments to define erosion rates. It is therefore premature to say that our tectonostratigraphic observations, while useful, would be able to conclusively indicate modifications relevant to the convective nature of the crust.

The radial Love number, h_2, would be an interesting additional physical parameter to study. This parameter represents the degree 2 change in the global height of a body given a specific tidal perturbation, is more sensitive to changes as a function of structure than k_2 is, and can be measured easily with an orbiter mission. Additionally, the thick atmosphere is a time-variable load on the surface of Titan and would provide geodetic signals at a different frequency than tides from Saturn. For terrestrial bodies, a joint analysis of both tidal and load (k_2' and h_2') Love numbers at varying frequencies can be used to investigate the dissipative properties of the body and provide a tighter

constraint on the structure of the body (Petricca et al. 2023; Wagner et al. 2024). Independent measurements of both Love numbers can also yield insight into the rigidity and thickness of Titan's crust (Wahr et al. 2006), providing rheological insights that would serve future models of Titan's evolution and heat flux. However, THUNDER's mapping plan was not designed with h_2 optimization in mind, so some edits to the mission design might be necessary before THUNDER is able to fully recover this parameter.

3. OBJECTIVE 2: DETERMINE WHETHER TITAN'S MAJOR LIQUID HYDROCARBON BODIES ARE CONNECTED AND EXCHANGING MATERIAL WITH EACH OTHER THROUGH A SUBSURFACE RESERVOIR.

3.1. *Science rationale*

Titan is the only known celestial body (except for the Earth) with stable and long-lived surface liquid reservoirs. On Titan, these liquid bodies cover $\sim 1.1\%$ of the surface and are distributed asymmetrically about the poles, with the North polar region (>55°N) hosting the great majority of all known surface liquids through a collection of over 650 hydrocarbon lakes and three large seas: Kraken, Ligeia, and Punga Mare (Birch et al. 2017; Hayes 2016). By contrast, Titan's South polar region contains only a few known liquid bodies (Lunine & Atreya 2008; Wood et al. 2013), with the largest, Ontario Lacus, containing only about 1% the liquid volume of the smallest northern mare (Brown et al. 2008; Turtle et al. 2009; Wall et al. 2010; Hayes 2016). The South polar region also hosts four large paleoseas comparable in size to the northern seas (Wood et al. 2013; Birch et al. 2018). This asymmetry may be due to orbital oscillations, similar to Earth's Croll-Milankovich cycles, which can enhance evaporation at either pole by driving changes in peak solar insolation (Aharonson et al. 2009; Lora & Mitchell 2015). Titan's south polar liquids may therefore have migrated northwards in the past ~ 45 kyr, leaving only Ontario Lacus as a remnant of its paleoseas (Birch et al. 2018).

Even if the evaporative effects of such cycles on either pole are expected to be similar, mapping done by Cassini's RADAR indicates a significant difference in their liquid-hosting potential, with the total (mostly empty) basin volume in the south polar region exceeding that of the (mostly filled) northern basin volume, though neither volume is well-constrained (Birch et al. 2017, 2018). The excess liquid required to reconcile this difference may reside in a substantial subsurface hydrocarbon alkanifer connecting its northern lakes and seas, analogous to aquifers connecting Earth's groundwater systems. Some investigations into lacustrine and sea properties based on RADAR backscatter and altimetry provide preliminary evidence for this alkanifer, such as the network of rounded lakes observed to exhibit seepage morphology with no obvious surface channels or shoreline evolution (Hayes et al. 2008), as well as certain surface elevation and compositional patterns as a function of distance to the large mare (Hayes 2016; Hayes et al. 2017; Birch et al. 2017; Mastrogiuseppe et al. 2019), though studies of shoreline morphology and basin depth are restricted by the limited range of Cassini's highest-resolution coverage ($\sim 40\%$ globally with HiSAR). Other supporting evidence for a groundmethane system on Titan comes from the liquid methane and ethane that were both identified in the porous regolith at the landing site of the Huygens probe (Niemann et al. 2005; Lorenz et al. 2006; Niemann et al. 2010).

This groundmethane system would play a central role in the long-term transport and exchange of hydrocarbons on regional (Turtle et al. 2018) or potentially global scales, accounting for as much as $\sim 1/3$ of influx into Titan's northern lakes (Horvath et al. 2016). Prevalent subsurface channels connecting its liquid bodies will also have significant implications for Titan's dynamic habitability. As the sharp, raised edges seen surrounding many of Titan's lakes nearly preclude pervasive lake-to-lake surface channels (Burr et al. 2013a; Poggiali et al. 2016; Birch et al. 2017), subsurface channels may be the only mechanism to transport highly complex organics across both its lakes and seas. Critically, these subsurface liquid hydrocarbons may then be in contact with the potentially porous ice shell (Horvath et al. 2016), which could facilitate exchange with Titan's suspected subsurface liquid water ocean and hence create potentially prebiotic environments. THUNDER's extensive coverage of Titan's polar wetlands will probe both indirect and direct evidence of such a large-scale subsurface reservoir.

3.2. *Physical parameter: Liquid body elevation*

If Titan's northern liquid bodies are indeed connected in the subsurface, then their relative surface elevations should reflect the height of the subsurface "methane table" in a manner that is significant against natural or random patterns in surface topography. Specifically, neighboring lakes and seas should share an equipotential surface wherein elevations of neighboring bodies,separated by ≤ 100 km, should commonly be within ≤ 5 m of each other and be less than the

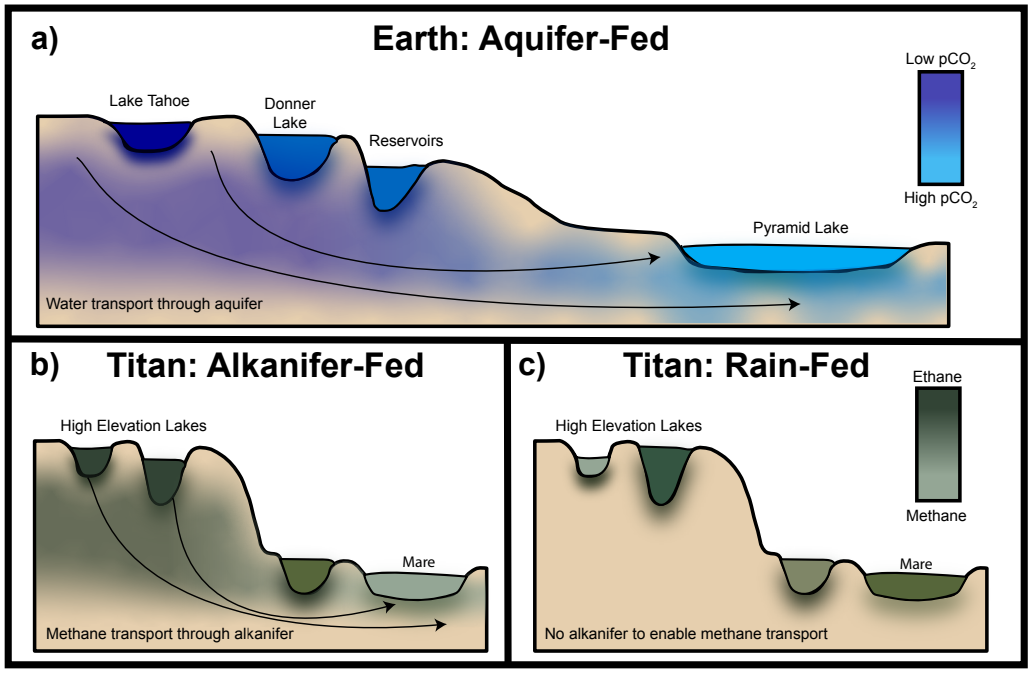

Figure 6. Panel a): Comparison of the elevation and composition gradients for the Truckee River System spanning California and Nevada, USA on Earth and panels b) and c): those comprising the two potential end-member scenarios for lakes in Titan's North polar region. The Earth analog for Titan's subsurface ethane-methane clathrate substitution is subsurface chemical processing resulting in enhanced pCO_2 levels downstream.

measured geoid height variation of 11 m across the lacustrine regions surrounding Kraken Mare and Punga Mare (≈ 1.5 m at 1σ; Iess et al. 2012; Hayes et al. 2017). Such an equipotential has been confirmed by Cassini altimetry between Kraken Mare and Punga Mare, though the relative surface height of Ligeia Mare is much less certain (Hayes 2016; Hayes et al. 2017). Further, empty lake basin floors should strictly lie at higher elevations than their surrounding lakes (or seas), as was seen in a limited number of Cassini flybys (Hayes 2016). In order to derive a robust conclusion, THUNDER altimetry will measure surface elevations with sub-meter precision for a statistically large sample (> 25) of neighboring lake pairs at a variety of distances relative to the maria. In addition to the relative surface elevations of neighboring lake pairs being lower on average (difference ≤ 5 m) than randomly-paired lakes, their distributions should be statistically distinct. Note that we consider only the relatively deep ($\gtrsim 10$ m), non-ephemeral lakes in this study; ephemeral lakes are expected to be shallow and rain-fed with minimal potential for subsurface exchange and differing structural dynamics (Steckloff et al. 2020).

On more regional scales, the surface elevations of lakes that are progressively closer to either of the three maria should exhibit a significant negative gradient if they are interconnected. Preliminary evidence for such a pattern was found in the handful of altimetric profiles that Cassini obtained with sufficient resolution and coverage over Titan's clustered lakes (Hayes et al. 2008; Hayes 2016; Mastrogiuseppe et al. 2019). Negative lake-to-mare gradients measured at the level $\geq 0.001\%$ for several chains of lakes would present a strong case for connectivity, by analogy with terrestrial hydraulic gradients in non-mountainous terrain (e.g., 0.012% for the Mississippi River, Wang & Morton 2022; 0.0047% for the St. Lawrence River System, US Army Corps US Army Corps of Engineers 1999). Figure 6 illustrates both distinct end-member scenarios for the surface elevations of Titan's liquid bodies, featuring the Truckee River System as a baseline for liquid body connectivity. While both tidal forces raised by Saturn and surface winds may drive fluctuations in measured liquid surface elevations, the expected amplitude of such effects is negligible relative to the topographic variation observed across the North polar region by Cassini (Corlies et al. 2017), even for Kraken Mare, which experiences the largest tidal range (≈ 50 cm; Tokano et al. 2014) and wind set-up (maximum ≈ 20 cm; Tokano & Lorenz 2015).

3.3. *Physical parameter: Polar liquid volume capacities*

As subsurface reservoirs may store liquid that formerly resided in now-empty southern basins, the existence of a substantial subsurface reservoir connecting Titan's lakes and seas may be inferred if the suspected polar liquid volume asymmetry is confirmed after northern and southern basin mapping is complete. If this interpretation holds, then the difference between the total southern basin capacity and total northern liquid inventory would indicate the scale of this groundmethane network. Current constraints from Birch et al. (2018) place a lower limit of 44,000 cubic km on the polar volume difference, though the uncertainty on the northern volume is $\sim 50\%$ and only upper limits have been estimated for the southern basin volume ($\lesssim 200,000\,\mathrm{km}^3$). In the North, it is expected that the three major mare, which are hundreds of kilometers in radius and reach depths well over 100 m, occupy $> 80\%$ of the total liquid volume (Hayes et al. 2008; Mastrogiuseppe et al. 2014; Hayes 2016; Mastrogiuseppe et al. 2018; Poggiali et al. 2020). Therefore, the greatest source of the uncertainty in the northern volume is the unknown bathymetry of these seas, particularly Kraken Mare, which is not only the largest but likely the deepest of the three (Mastrogiuseppe et al. 2018; Lorenz 2021; Miller et al. 2021). In the South, the total volumetric capacity is analogously dominated by the four paleosea basins (rather than the many paleolakes, Lopes et al. 2019a), making the determination of their elevation profiles crucial. This is particularly true for the unmapped regions of Buzzell Planitia Basin (e.g., see Birch et al. 2018), whose true size may only be estimated with additional SAR measurements. Hence, with THUNDER's expanded radar coverage, we will calculate both polar volumes to much greater precision by completing radar mapping in SAR and altimetry modes over both the northern seas and southern paleoseas. Cassini altimetry yielded high uncertainties over the southern basins, and the Ku-band saturated before reaching the depth of large Kraken Mare (Poggiali et al. 2020). We therefore cannot understand the total volume of liquid on Titan, or its distribution, without a wider survey of Titan's empty basins and deeper-penetrating radar frequencies over filled mare.

As is the case with surface elevations (Section 3.2), liquid volumes on Titan are modulated by tides, winds, and precipitation. Tidal forces may facilitate $\sim 20\,\mathrm{km}^3$ of liquid exchange per Titan day between Kraken Mare's northern and southern basins and perhaps a few km^3 between the surface-connected Ligeia Mare and Kraken Mare (Lorenz et al. 2014; Tokano et al. 2014). Wind-driven circulation may drive somewhat more significant exchange ($\approx 7\,\mathrm{km}^3$) between Ligeia Mare and Kraken Mare, but over a much longer timescale, spanning the entire northern summer (Tokano & Lorenz 2015). These mechanisms, therefore, produce only minor ($< 1\%$) fluctuations in volume that translate to only small surface elevation and shoreline changes (< 1 m for Kraken Mare, well below the spatial resolution of THUNDER's SAR; Tokano et al. 2014). Similarly, the volumetric contribution from precipitation should be negligible; assuming an extreme upper limit of ≈ 100 mm of rainfall over the course of THUNDER's prime mission covering an area $3\times$ that of the sea surfaces ($\approx 2 \cdot 10^6\,\mathrm{km}^2$; Hayes 2016), the contribution of rainfall is limited to $\lesssim 200\,\mathrm{km}^3$, which is $< 0.3\%$ of the total northern surface inventory. Liquid volume capacities measured by THUNDER can therefore be considered reasonably static over the course of the mission, although repeated measurements will be taken in order to validate observations.

3.4. *Physical parameter: Specific attenuations of liquid bodies*

If Titan's liquid bodies are connected in the subsurface, then neighboring lakes should have comparable compositions due to chemical equilibration (similarly to their surface elevations, see Section 3.2). Additionally, the presence of a subsurface clathrate layer (Choukroun et al. 2010; Choukroun & Sotin 2012) could cause lakes to exhibit progressively higher methane:ethane ratios with proximity to the large seas. The logic is as follows: Subsurface channels connecting Titan's liquid bodies are likely to be in contact with clathrate cages, which preferentially trap liquid ethane and release captured methane (Choukroun & Sotin 2012; Mousis et al. 2014). Lakes at the furthest distances and highest elevations relative to the seas should primarily be rain-fed, while the lower-lying lakes nearest to these seas receive significant subsurface replenishment. Therefore, more 'mature' lakes at lower elevations, which tend to be closest to the seas, will naturally have higher methane-ethane mixing ratios.

The true concentrations of these bodies' constituents are highly uncertain with currently available data (Mitchell et al. 2015; Le Gall et al. 2016; Mastrogiuseppe et al. 2019). We will use THUNDER altimetry to obtain the specific attenuation of Titan's lakes and seas, which we will use as a proxy for the relative methane and ethane content of Titan's liquids. While the SAR backscatter (reflected intensity σ_0, often in dB scale) is strongly dependent on a body's methane:ethane ratio (the difference in reflectivity between pure methane and ethane is > 2 dB in the Ku band;Mastrogiuseppe et al. 2019). Cassini SAR revealed that lakes further from the seas generally have lower reflectivity (Birch et al. 2017), while altimetry was sufficient only to derive the specific attenuation for two seas (Ligeia

Mare; Mastrogiuseppe et al. 2014, 2019 and Punga Mare; Mastrogiuseppe et al. 2018) and one lake (Winnipeg Lacus) at an intermediate distance to the seas, finding the lake to be slightly less methane-rich than Ligeia Mare (Lorenz 2014b; Mitchell et al. 2015; Mastrogiuseppe et al. 2019). Higher-resolution altimetric and SAR coverage will allow us to probe the attenuation across lakes and seas of sizes >300 m in diameter.

If subsurface alkanifers connect lakes, neighboring lake pairs should have more similar specific attenuations (slopes within $\approx 1\mathrm{dB}\,\mu\mathrm{s}^{-1}$;Mastrogiuseppe 2019) than random pairs. Due to expected chemical modulation by precipitation, random pairs should be selected in regions that receive comparable rainfall amounts, such as at similar latitudes– e.g., within about $< 2^\circ$ in latitude, where methane mole fractions should vary $< 1\%$ due to rainfall (Tokano & Lorenz 2016). While Punga Mare, Ligeia Mare, and the northern portions of Kraken Mare ($> 75^\circ$N) should generally be methane-rich, there is no clear prediction for their relative specific attenuations as surface channels (expected to largely flow from Punga Mare → Ligeia Mare → Kraken Mare) may dominant inter-mare exchange (and are expected to enhance ethane concentration down-flow; Lorenz 2014b; Tan et al. 2015; Lorenz 2021).

3.5. *Measurement requirements*

An overview of the spatial coverage for Objective 2 is provided in Figures 9 and 10. THUNDER will make use of its radar instrument in SAR, altimetry, and radiometry modes as well as its visible-to-infrared (vis-IR) spectrometer to achieve complete and nearly continuous coverage of Titan's polar wetlands. THUNDER's near-polar orbit, described later in more detail in Sections 6.2 and 7.1, means that each individual transect will strongly vary in latitude, but follow a line of near-constant longitude. However, the many transects planned over the course of its prime mission will sample a wide range in longitude, allowing THUNDER to capture a large number of lakes spanning a range of distances to the seas at any given latitude, and also enabling latitudinal biases in attenuation and elevation to be well characterized. 100 m/px spatial resolution in SAR mode enables identification and imaging of lakes with radii down to a few kilometers. This will allow us to identify $\approx 99\%$ of Titan's filled and empty basins based on estimates from Cassini-resolution data (Hayes et al. 2008; Hayes 2016). 20 cm vertical altimetry precision supports measurements of surface elevation, depth, and specific attenuation for such small, relatively shallow bodies. As THUNDER's low-frequency X-band altimeter will also penetrate deeper than Cassini's Ku-band altimetry, which was sufficient to detect echoes returned from depths of > 100 m (and 170 m in the case of Ligeia Mare; Mastrogiuseppe et al. 2014), its altimetry should be able to detect seafloor echoes for most of Titan's lakes and seas (although the current depths are not resolved for the deepest liquid bodies, maximum depths should not exceed ≈ 300 m; Lorenz et al. 2014; Tokano et al. 2014; Le Gall et al. 2016; Lorenz 2021), including those inaccessible with Cassini (e.g., portions of Kraken Mare and a few other lakes; Mastrogiuseppe et al. 2018, 2019; Poggiali et al. 2020). Passive radiometry obtained simultaneously in SAR and altimetry modes, which is highly sensitive to variations in Titan's surface brightness temperature (~ 0.1 K changes, e.g., Elachi et al. 2005; Paganelli et al. 2008; Janssen et al. 2009, 2016), will help to identify evidence of recent rainfall events on large scales ($\gtrsim 100$ km). Wide and high-cadence coverage with THUNDER's high-spectral-resolution vis-IR spectrometer will provide more robust detection and detailed characterization of surface wetting down to smaller scales of $\gtrsim 5$ km, via broad specular reflections in several windows from 1–3 μm (Barnes et al. 2013; Dhingra et al. 2019, 2020).

Across Titan's North polar region ($> 55^\circ$N), THUNDER will need to perform roughly two dozen independent transects. Each transect will feature vis-IR and radar coverage in all three modes, requiring at least 2 orbits. THUNDER will first focus on observations of Titan's lakes, which are most susceptible to seasonal evolution (see Section 5), passing through the dense lake cluster centered at 77°N, 142°W , half of which will also cover the relatively dense region bounded by Neagh Lacus, Ladoga Lacus, and Bolsena Lacus. The other half of these transects will cross the northwest and northeast portions of Ligeia Mare and Kraken Mare, respectively, providing a direct connection between chains of lakes and seas. THUNDER will then map transects connecting Punga Mare with the eastern lakes scattered across $\approx$ 40–120°W and with the two other seas, Ligeia Mare and Kraken Mare. Additional transects will also directly connect the central and eastern portions of Ligeia Mare to a collection of lakes in the range, and cover the sparser groups of lakes found at latitudes of 70–85°N near $\sim$ 200°W and $\sim$ 50°W, respectively. In the South ($> 55^\circ$S), THUNDER need only cover the four large paleoseas (to estimate the liquid volume capacity), which can be accomplished via ≈ 10 transects constituting three sets of 3–4 transects across Buzzell Planitia Basin, Ontario Lacus Basin, Romo Planitia, and Rossak Planitia Basin.

3.6. *Some challenges and future areas for study for Objective 2*

This objective does not fully account for the range of processes that may be modulating observable physical parameters of Titan's surface liquids. First, the composition of groundmethane will be affected by the properties of the crust, which, as also discussed in Section 2.6, are not explicitly measured in this mission. If the crust has a high porosity, which would be necessary for storage of the subsurface alkanifer, clathratization should be somewhat rapid (Hayes et al. 2008; Choukroun & Sotin 2012). The clathratization rate may also change as a function of depth and therefore temperature (Vu et al. 2020), while this objective considers a somewhat binary existence of a subsurface reservoir rather than raising possible variations in storage with depth. To this end, we note that our expectations for subsurface transport are over-simplified. For example, flow towards the major seas may be disrupted by local topographic minima and ultimately regulated by different drainage basins (Hayes et al. 2017), which would produce elevation and chemical gradients on smaller scales than expected. The relationship between clathrates, composition, and total liquid volumes thus depends on the porosity, permeability, and composition gradient of Titan's icy crust; all of these factors are, in turn, modulated by the unknown thermal structure discussed in Objective 1.

A subsurface, polar liquid reservoir would also likely be open for atmospheric exchange (Turtle et al. 2018), so the properties of the liquid will reflect atmospheric and seasonal cycles in complex ways. Seasonality is discussed in more detail in Section 5, but solar insolation should gradually decrease throughout the mission, possibly cooling surface temperatures as well as lakes and seas. Furthermore, if ethane is preferentially trapped in clathrates and therefore removed from subsurface liquids as they travel towards basins, such that the composition of basins in the polar region is more methane-rich, as we suggest, it will affect surface pressure and enhance methane-rich rainfall (Mousis et al. 2016). Importantly, coupled with decreasing precipitation (which acts to strengthen liquid density gradients) throughout autumn (Tokano 2009; Schneider et al. 2012; Tokano & Lorenz 2016), this cooling may be sufficient to induce overturn and allow Titan's liquids to mix later in the mission timeline (see Section 5), modulating the methane:ethane ratio of liquids entering the subsurface. This effect cannot be well-characterized due to uncertainties in the properties of the subsurface, including the height of the methane table, which determines subsurface infiltration dynamics (Hayes et al. 2008; Horvath et al. 2016). Raindrops may also be more ethane-rich than expected (with ethane mole fractions as high as 40%; Graves et al. 2008), and pure ethane precipitation is expected to intensify towards winter (Lorenz 2014b; Tokano 2021), elevating the likelihood of overturn in Titan's lakes and seas and therefore biasing THUNDER's ability to measure composition. At 91 K, a stratified lake experiencing such an event should, however, remain stable against overturn since the relatively methane-rich rain would strengthen its vertical density gradient (Malaska et al. 2017). On the other hand, the lake's bulk methane content would be enhanced, lowering its observed specific attenuation. This effect may be exaggerated for deep or ethane-rich lakes since altimetric echoes that do not reach the sea floor will be attenuated by their relatively methane-rich upper liquid layers.

Finally, even if the above effects are sufficiently accounted for, more laboratory experiments involving Titan's ternary fluids under relevant conditions are needed to interpret the data from THUNDER (e.g., involving their interaction with solid/icy hydrocarbons in the subsurface, or characterizing their X-band reflectivity/attenuating properties).

4. OBJECTIVE 3: DETERMINE IF TITAN IS LOSING ITS ATMOSPHERE AND SURFACE LIQUIDS

4.1. *Science rationale*

Titan's methane hydrological cycle is unique in the Solar System, but it is unclear whether the nitrogen- and methane-dominated atmosphere is a permanent feature of Titan, or if methane is lost without replenishment over geologic time. Hydrogen in Titan's atmosphere is quickly lost to space following methane photolysis, and methane is irreversibly consumed by the processes which generate hazes, complex organics, and potentially-prebiotic molecules observed from Earth and by Cassini-Huygens (Lunine & Atreya 2008). Thus, the atmosphere is expected to collapse within <30 Myr without sources of methane and hydrogen gas to replenish the atmosphere (Hörst 2017). Without an identified source of methane recharge, it is therefore possible that the atmosphere is recent.

We suggest that the global morphology of Titan's surface, while also relatively young, is the best indicator of whether material loss or stabilizing replenishment dominates over long timescales. We aim to determine whether the surface records the presence of an ancient global surface ocean (Figure 7) and interpret what the extent of such a past ocean can tell us about the balance of loss and replenishment of surface liquids and of atmospheric materials. If Titan once hosted a vast surface hydrocarbon ocean, as suggested in Larsson & McKay (2013), the lakes and seas that we see today would serve as the last remnants of this ocean, which would have decayed through time as its evaporation fed the atmosphere. Presently, only ∼2% of Titan's ice shell is covered in hydrocarbon liquid, nearly entirely at the poles (Lopes et al. 2019a). If a global ocean existed, we may now be seeing Titan as a world in the midst of extreme climate

change, as the last of its liquid methane reservoirs are exhausted. The rate of evaporation would necessarily accelerate through time, as the icy surface became more exposed, such that the Titan we see today might be rapidly changing over geologic time. This knowledge has the potential to transform our view of Titan as a potential habitable locale – if Titan is actively losing material, then supply of prebiotic chemicals into hospitable environments cannot be sustained indefinitely – and will allow us to better understand the breadth of potential fates for similar worlds like Triton and Pluto.

Figure 7. Two possible scenarios of Titan's liquid coverage at roughly 1 Gya. Black is liquid coverage, and color shows exposed ice shell and its relative elevation, where dark red indicates higher elevation and dark blue indicates lower elevation. On the left is the scenario wherein Titan was covered by a global hydrocarbon ocean in the past, and has since lost liquid coverage to reveal the surface seen today. Alternatively, if the body has not been losing surface liquids, the coverage would have been stable for the past 1 Ga. (Adapted from Larsson & McKay 2013)

4.2. *Physical parameter: Current and past lake depths*

We will first investigate whether Titan's hydrocarbon-rich atmosphere is a permanent feature by comparing recent-past and present liquid surface inventory. The atmospheric methane content is at least seven times that of surface liquids, indicating that atmospheric changes exert control over lacustrine bodies rather than vice versa (Hayes 2016); we therefore can use lake depths past and pressent as an indicator of atmospheric stability.

Similarly to the process described in 3.2, we will use altimetry and SAR to measure both the northern and southern regions for the current liquid depths across the course of the mission. THUNDER's global surface mapping will allow comparison of lacustrine volumes over a period of 4.5 years (THUNDER's science orbit) and over roughly 1 Titan year (between measurements taken by Cassini and comparable measurements taken by THUNDER). The Cassini mission may have seen evidence of extreme lake level change in Ontario Lacus (<10 km; Turtle et al. 2011) over the course of a five-year span; Hayes et al. (2011) also reported disappearance of lacustrine features over a two year period which can only be explained by ground infiltration or evaporation. By tracking combined North and South polar lake volumes between Cassini and THUNDER, and over the course of THUNDER's science operations period, we can determine whether extreme variations are interannually repeatable, related to seasonality, indicative of pole-to-pole transport, and/or caused by net material loss phenomena.

We will also conduct extensive mapping of the south polar region, where paleoseas may have once held much of Titan's methane (Birch et al. 2017, 2018). Using SAR and altimetry, we can ascertain shoreline extents and calculate basin depths, oscillating variations of which can elucidate the extent of interannual or seasonal changes (Faulk et al. 2020). It may be possible to observe evidence of past shoreline erosion in southern basins (Palermo et al. 2024; Hayes 2016), which could also be indicative of previous liquid levels. Currently, the majority of Titan's surface liquids are found in the North polar region, likely due to orbital forcing. If paleoshorelines can be found beyond the extent of the current shorelines of northern liquid bodies, this would indicate that the total liquid volume on the surface was greater during previous Croll-Milankovitch cycles ($\sim$ 45 kyr periods; Aharonson et al. 2009) and has since been lost.

If the total surface liquid volume and distribution remain constant over time, this would indicate that either change in volumes are too slow to observe on the timescale of the THUNDER mission or that loss and replenishment are approximately balanced. The same is true if the total volume is constant but the distribution shifts from pole-to-pole. A longterm increase in total volumes, while unexpected, may suggest replenishment from subsurface reservoirs or outgassing. Finally, a net decrease in total standing liquid on Titan's surface would indicate a loss of liquid to the atmosphere or subsurface. The extent of liquid loss over a certain period of time could be compared to required methane replenishment to the atmosphere to compensate for loss due to the known photolysis rate.

4.3. *Physical parameter: Crater size and depth*

In order to sustain an atmosphere of consistent methane density, and therefore of similar strength, over time, Titan may have hosted a massive global hydrocarbon ocean on its surface over its history. If this ocean existed, the poles and other unprotected topographic lows which were covered the longest should be relatively crater-poor, while high elevation terrain at low latitudes should have been more intensely cratered prior to erosion and infill. The subsurface ocean, which is likely water-dominated (MacKenzie et al. 2021), is not a sufficient reservoir to replenish any methane that has disappeared from the atmosphere and surface. Additionally, subsurface methane reservoirs, like those studied

in THUNDER's Objective 2 (Section 3), may be invoked as sources for atmospheric methane replenishment or storage of past surface liquids. However, the estimated equivalent liquid volume of methane lost over 1 Gya given a constant photolysis rate is ∼1.32 x 10^7 km^3 (Tokano 2023). This volume far exceeds the estimated capacity of known surface and subsurface reservoirs (∼200,000 km^3; Hayes 2016; Birch et al. 2018). Thus, it is possible that methane could have been stored both in subsurface reservoirs and an extensive surface ocean.

At 1 Gya, this hypothesized hydrocarbon surface ocean would have covered roughly 50% of Titan's surface at maximum (Larsson & McKay 2013; Tokano 2023), with exposed highland material mainly concentrated at the equator. Even at only 300 Mya this global ocean would have covered 25% of the surface and flooded regions near the equator. Since data from Cassini indicate that the age of the equatorial surface is at least 500 Myr and Titan's crater retention age may be up to 1 Gyr (Neish & Lorenz 2012; Neish et al. 2016; Rossignoli et al. 2022), the surface is young enough to still retain evidence of differing cratering rates between regions covered and not covered by this potential past ocean. In particular, the equatorial and ∼35°latitudes, which contain some of the oldest terrain on Titan, will be of importance to address this science objective.

The crater catalog available from Cassini RADAR supports differing cratering rates in topographic highs and lows (Neish & Lorenz 2014), but Cassini only covered 46% of Titan's surface in >1 km/px resolution (with an additional 24% covered by >5 km/px resolution) (Lopes et al. 2019b). The unmapped and low-resolution regions overlap significantly with highlands and sheltered lowlands that would theoretically have been exposed a billion years ago, so we are presently unable to determine the relative age of those regions. We expect that these highlands should retain significant cratering, and that more advanced mapping of low topography and polar regions should not reveal elevated crater counts. Since erosion and infill processes erase crater morphology, particularly for ancient craters, vis-IR measurements are critical for comparison of crater bottom compositions with evaporite and with known and expected crater bed compositions to understand the extent to which various craters have been modified, and therefore for relative crater dating.

THUNDER's extensive vis-IR coverage allows us to differentiate signs of chemical weathering from variations in the composition of underlying material. During this investigation, evidence for fluvial erosion in newly discovered craters, such as rims and ejecta blankets enriched in water ice and insoluble organics (Neish et al. 2015), will be sought, to determine whether such a process is global (Neish et al. 2016). Additionally, erosion rates and processes are not expected to be constant with latitude, due to, for example, differences in permeability (Horvath et al. 2016; Faulk et al. 2020). Thus, the global ocean hypothesis will be tested by considering regions at similar latitudes.

4.4. *Measurement requirements*

In order to measure liquid volumes, THUNDER will use altimetry and X-band SAR. This radar bandwidth will allow the instrument to penetrate to the bottom of the deepest northern lakes and seas (unachievable with the Ku-band radar used on Cassini; Mastrogiuseppe et al. 2019; Lorenz 2021). Observation in both SAR and altimetry modes for polar regions northward of 55°at all longitudes and over Ontario Lacus, which overlaps with the coverage required for Objective 2, is necessary to obtain volume estimates for both northern and southern lakes and track the total surface liquid volume over time (see Figure 9). SAR mapping with $\leq$ 1 km spatial resolution and altimetry with $\leq$ 1 m vertical precision is required in order to constrain lacustrine volumes, and in order to measure any interannual variations $\lesssim$ 10 km shoreline retreat (comparable to that possibly seen over the course of the Cassini mission; Turtle et al. 2011). Additional SAR and altimetry coverage of the equatorial regions from 45°S to 45°N near the Senkyo region and the Xanadu region is required for a comprehensive crater survey of Titan's highlands and lowlands.

SAR resolution of $\leq$ 500 m/px will enable THUNDER to expand the Titan crater count inventory to include craters <2 km in diameter, where there are currently few verified craters (Hedgepeth et al. 2020). Radar altimetry with $\leq$ 500 m along-track resolution and $\leq$ 10 m vertical precision will allow for profiling of those small craters. Radiometry with $\leq$ 150 km area pixels and $\leq$ 0.75 K brightness temperature precision will be used to ascertain the amount of surface wetting in cratered areas and infer from this the extent of erosion and infilling. Emissivity values obtained from radiometry can provide information about the presence of potential clathrates, which would give higher emissivity than regions with higher amounts of water ice. Radar-dark equatorial regions may also indicate materials deposited following storms; Neish et al. (2015) assert that chemical erosion is an important process at low latitudes, but since rainfall is likely quite infrequent and sporadic, it is difficult to ascertain how this translates to overall erosion rates without more continuous monitoring. Finally, vis-IR with $\leq$ 10 km spatial resolution and $\leq$ 25 nm spectral resolution in the wavelength range 0.94 - 3.2 µm is necessary to constrain the degree of infilling by comparing observed spectra from crater bottoms to experimentally determined crater bottom compositions and to evaporite signatures (Solomonidou

et al. 2020). Due to the precession of THUNDER's science orbit, overlapping adjacent ground swaths will be covered by the vis-IR with a temporal separation of at least 1.7 years, which allows effectively permanent deposits to be discerned from transient features such as clouds or wetting from recent rainfall.

4.5. *Some challenges and future areas for study for Objective 3*

This objective, as written, aims to constrain the longevity of Titan's atmosphere, but in its above form offers only a look at current surface conditions. The measurements proposed for this objective and the first physical parameter would indeed change our understanding of the surface liquid budget of Titan, but are incomplete to address the atmospheric aspects suggested. For example, current liquid levels may be affected by tidal forcing timescales, which can move liquid between bodies (Tokano et al. 2014), while the extent of recent rainfall is a function of seasonality and can strongly influence local properties like reflectivity (discussed in greater detail in Sections 3.2 and 5). Additionally, while comparisons to Cassini data, as suggested in Section 4.2, would be ideal for evaluating timescales of change, the approach we describe fails to account for any process of surface modification other than liquid evaporation, and does not necessarily provide strong constraints on the extent of change expected. Section 5 provides a more thorough overview of the effect of temperature, precipitation, and seasonality on THUNDER's ability to achieve this proposed objective.

As discussed in 2.6 for Objective 1, both the crustal composition and the dominant erosional mechanisms of Titan's surface are presently unknown, which would not be remedied by the current presentation of this mission. Crater counting in the absence of crater removal or infill timescales, and without constraints on the relaxation rate of the crust, is not a viable mechanism to explore the history of atmospheric effects on the surface. Instead, this physical parameter may best be coupled with detailed mapping in vis-IR in order to assess the extent of chemical crater erosion, which was observed in three craters by Neish et al. (2015), vs. fluvial erosion (Neish et al. 2016) or infill, across Titan's climactically variable surface. A new objective which aims to constrain the dominant mechanisms and erosion rates on Titan's surface, possibly restated as "Determine whether Titan's craters are dominantly modified through material removal, crustal relaxation, or material deposition," would also complement Objective 1 (Section 2). This new objective would then be able to address atmospheric concerns, as measuring the competing rates of the three proposed mechanisms would better constrain the contribution of the atmosphere to surface modification.

5. COMMENTARY ON TITAN SEASONALITY

The volumes and compositions of Titan's surface liquids, important for Objectives 2 and 3, are highly dependent on seasonality. Per the mission trajectory described in section 7.1, THUNDER will achieve Titan Orbit Insertion during late northern summer, at which point it may begin preliminary science measurements (at solar longitude $L_s \approx 135°$). THUNDER will subsequently reach its nominal science orbit near the onset of autumn ($L_s \approx 150°$), and continue its primary mission through northern autumnal equinox, concluding in as little as 3.6 Earth years ($L_s \approx 200°$) and as many as 4.6 Earth years ($L_s \approx 210°$). Here, we summarize some potential changes to surface and liquid properties that may occur over the course of the mission.

First, Titan's temperature will change as we observe through autumn. In the North polar region, which is generally 2–4 K cooler than the equatorial regions (Schinder et al. 2011; Schneider et al. 2012), solar insolation will be moderate but gradually decreasing throughout this ≈ 4-year primary mission. Diurnal surface temperature variations (i.e., over 1 Titan day or 15.9 Earth days) as large as 1.5 K have been recorded at low latitudes, but show a tentative decrease in magnitude towards the poles and may be negligible poleward of ±60° (Cottini et al. 2012). Based on measurements from Cassini spanning northern winter to early summer, we can expect that average surface temperatures in the North polar region will only cool by ≈ 0.5 K (remaining near 92 K) from late northern summer to late autumn (e.g., Jennings et al. 2011; Cottini et al. 2012; Le Gall et al. 2016).

Models indicate that the surface layers of methane-rich lakes and seas should be relatively temperature-stable during THUNDER's observation period, however. Their surface layers should generally remain 1–2 K cooler than surrounding land (near 91 K) and their underlying vertical structures should be highly stratified, featuring methane-rich upper layers and ethane-rich lower layers, following the end of summer (Tokano 2009; Tokano & Lorenz 2016; Malaska et al. 2017). Sea levels are also expected to be near maximum levels upon THUNDER's arrival and should generally be stable, perhaps decreasing by a few tens of cm over the course of the prime mission (Tokano 2009).

Seasonal changes to sea levels are largely driven by decreasing precipitation, which is a primary driver of Titan's fluid evolution and strong control on the observable extent of surface liquids. Observations of cloud cover (Schaller

et al. 2006; Turtle et al. 2009; Rodriguez et al. 2009) and fluvial features (MacKenzie et al. 2014) from Cassini, as well as climate models (Tokano 2009; Schneider et al. 2012; Tokano & Lorenz 2016), suggest that Titan's precipitation cycle in the North polar region peaks near summer solstice and will be relatively active, but waning, throughout autumn. Precipitation rates are expected to be a strong function of latitude, increasing sharply towards the poles (Tokano 2009; Schneider et al. 2012; Lorenz 2014b), which may result in naturally elevated sea levels at higher latitudes. Models indicate, however, that maximum rainfall totals over the summer season should not exceed $\sim 50\,\mathrm{mm}$ (Lorenz 2000; Barth & Toon 2006; Rannou et al. 2006), which is well within our 1 m elevation tolerance for neighboring liquid bodies and negligible relative to regional topographic changes. As such, even if an extreme rainfall event (or cyclone, e.g., Tokano 2013) producing a Titan year's worth of precipitation ($\approx 100\,\mathrm{mm}$) occurs during THUNDER's operations, our surface elevation investigations for Objectives 2 and 3 would not be compromised.

In addition to influencing sea levels and volumes, precipitation affects overturn, liquid composition, circulation, and vertical stratification. Being more volatile than ethane, methane will preferentially evaporate out from Titan's seas (Malaska et al. 2017) and should primarily constitute Titan's precipitation cycle throughout northern summer and autumn (Lunine & Atreya 2008; Niemann et al. 2010), regardless of latitude (Cordier et al. 2012), though drops may partly be comprised of nitrogen (with methane-nitrogen mixing ratios of $\approx 4:1$ Graves et al. 2008; Malaska et al. 2017). We note that pure ethane precipitation may originate from higher in the troposphere (Rannou et al. 2006; Griffith et al. 2006; Tokano 2021), but its total ground flux should be negligible compared to methane rain, especially outside of winter (Lorenz 2014b), so we ignore its contribution in this discussion. Evaporation of methane is non-continuous (Brown et al. 2009), but generally should occur more slowly than precipitation throughout THUNDER's mission, except towards the end of autumn when they are expected to fall in balance (Tokano 2009; Tokano & Lorenz 2016).

Like precipitation, surface winds act to cool Titan's liquid bodies and will also be operating at moderate (but waning) intensity throughout THUNDER's mission, with average speeds of $\approx 0.5\,\mathrm{m\,s^{-1}}$ and $\approx 0.2\,\mathrm{m\,s^{-1}}$ in early and late autumn, respectively (Tokano & Lorenz 2015). Cooling induced by such winds is likely too weak to trigger overturn in Titan's stratified lakes, in part due to ongoing precipitation that will strengthen vertical density gradients (Tokano & Lorenz 2015). Stresses from winds may change the apparent roughness of Titan's liquid surfaces (i.e., create waves), but Cassini found that Titan's seas are remarkably calm (at least from winter to early summer) with RMS surface height variations less than a few mm over the major seas in late spring (Zebker et al. 2014; Poggiali et al. 2024). Winds may also drive currents (of order a few cm $\mathrm{s^{-1}}$) that cause liquid accumulation and heightened surface elevations near downwind shorelines, an effect known as "wind set-up". This effect is most significant for the largest seas and may drive substantive liquid exchange, potentially on the order of $7\,\mathrm{km^3}$ between Ligeia Mare and Kraken Mare and a few $\mathrm{km^3}$ between Kraken Mare's northern and southern basins during northern summer (Tokano & Lorenz 2015). Depending on where measurements are taken, elevation gradients could temporarily strengthen (in the case of negative set-up) or weaken (in the case of positive set-up), as these two seas are the presumed to be at the lowest elevations. THUNDER is capable of altimetry precision of 20 cm at its finest, so we will be able to capture the changes through repeat passes, thereby better understanding sea exchange and the total volumes of liquids necessary for answering Objectives 2 and 3.

6. PAYLOAD AND DATA COLLECTION

6.1. *Instrumentation*

THUNDER's instrument payload consists of a visible-to-infrared (vis-IR) spectrometer and a radar with three operational capabilities: synthetic aperture radar (SAR), altimetry, and radiometry. The instrument suite is complemented by a gravity science investigation, which makes use of the telecomms subsystem to enhance the science return of the mission. Specific information regarding instrument capabilities and payload accommodation requirements imposed by instrumentation are detailed in Table 1 and Table 2, respectively.

6.1.1. *Visible-to-Infrared Spectrometer*

The THUNDER vis-IR point spectrometer is patterned after the OSIRIS-REx OVIRS instrument. While Cassini VIMS only covered about 5% of Titan's surface with resolution <6 km per pixel (20% of the surface at <10 km per pixel resolution; Le Mouélic et al. 2019), the THUNDER vis-IR mapping will cover 42% of Titan's surface at finer than 10 km/px spatial resolution and 10 nm spectral resolution (Figure 10). This level of coverage is necessary to search for evidence of recent precipitation events in the vicinity of lakes and to correct volume and composition estimates

for Objectives 2 and 3 accordingly. Evidence of recent rainfall will be defined by enhanced specular reflectance within the same ground track using spectral bandwidths between 1.2 and 3.1 μm(Dhingra et al. 2019). Additionally, vis-IR spectral measurements between 0.94 and 3.2 μm are required to detect infill and constrain erosion timescales of highland and lowland craters down to 10 km in diameter via transmission windows in Titan's atmosphere (Corlies et al. 2021). Repeated coverage, especially overlapping measurements at high latitudes, will allow for differentiation between signatures from transient features, such as clouds and rainfall, and permanent features such as crater infill. Rather than increase integration time, additional time-binning (or, co-adding) on the ground is used to increase signal-to-noise ratios. The vis-IR spectrometer will generate 18.0 Gbits of data, driven largely by coverage necessary for Objective 3.

Table 1. Instrument capabilities compared to mission science requirements.

Instrument		Science Requirement	Instrument Capability	% Margin
Vis-IR Spectrometer	Spatial Resolution*	≤ 10 km	5 km	50%
	Spectral Bandwidth	0.93–3.2 μm	0.4-4.3 μm	23%
	Spectral resolution	≤ 25 nm	10 nm	60%
	SNR / wavelength	≥ 30:1	≥ 45:1†	50%
Radar - SAR Mode	Spatial Resolution*	≤ 125 m	100 m	20%
	Swath Width*	≥ 20 km	31 km	55%
	Sensitivity	–26 dB	–20 dB	30%
Radar - Altimeter Mode	Vertical Precision	≤ 1 m	20 cm	80%
	Along Track Resolution*	≤ 500 m	300 m	40%
	Swath Width*	≤ 10 km	6.0 km	40%
	Sensitivity	–20 dB	–22 dB	10%
Radar - Radiometer Mode	Resolution*	149 km	124 km	17%
	Sensitivity	0.75 K	0.6 K	13%
Gravity Science	Included in telecoms			

* At 1300 km altitude
† Includes time binning on ground

6.1.2. *Radar - SAR, Altimeter, and Radiometer Modes*

The THUNDER radar instrument with SAR, altimetry, and radiometry capabilities is based on the radar instrument from the 2008 Titan Explorer Flagship Mission Study (Lorenz et al. 2008; Applied Physics Laboratory 2008). That instrument in turn is based on the Delay-Doppler Phase-monopulse radar (D2P), which was the result of NASA Instrument Incubator Program (IIP) funding to JHU/APL. The 2 m X-band high-gain antenna (HGA) is shared between the radar instrumentation and telecommunication system. The X-band wavelength (8-12 cm) will provide new information on slightly larger-scale surface roughness in repeat coverage areas and allow us to penetrate the deepest lakes and seas, which was not possible using the Ku-band (2.18 cm wavelength) radar on Cassini.

In SAR mode, the HGA is pointed 30° off-nadir. We will be able to process radar data to $\leq$ 125 m/px resolution using standard Doppler delay techniques (Raney 1998), covering at least 83% of Titan's surface. This resolution, which is similar to that of high-altitude Huygens descent imagery (Figure 5), will achieve near-global coverage which allows for unambiguous identification of streambeds as they cross-cut faults and folds, producing the necessary mapping for constraining the relative ages of geographic features as required for Objectives 1 and 3. We will generate 340 Gbit total of data from SAR observations, driven by the coverage necessary for Objectives 1 and 3.

The altimeter mode, with a swath width less than 10 km and sharpened along-track to a resolution better than 500 m, will enable topographical measurements that allow for reliable differentiation between admittance models at low spherical harmonic degrees. Vertical measurement precision better than 1 m is required to constrain changes in lake

liquid levels over time using specular radar reflections in radar echoes. This will generate 14 Gbit total, driven by the requirements for Objectives 1, 2, and 3.

Radiometry may be operated simultaneously with SAR and altimetry. Changes to microwave emissions from the surface over areas smaller than theoretical size of Titan rainstorms (∼70,000 km^2 - 115,000 km^2; Dhingra et al. 2020), suggestive of temperature changes due to evaporation after rainfall, can be detected with brightness temperature precision better than 0.75 K. In order to assess these differences across given lakes in a region, THUNDER will collect radiometry data using dimensions of $\leq$ 149 km/px horizontal resolution. This will generate 14.4 Mbit of data, driven by requirements from Objectives 2 and 3.

6.1.3. *Commentary on Radar instrumentation*

Additional instrument concept studies (e.g., Mastrogiuseppe 2019) and funded missions (e.g. NASA's VERITAS mission; Hensley et al. 2020; Smrekar et al. 2022) have proposed or designed radar instrumentation with higher resolution and/or more capabilities than those selected for THUNDER. Here, we briefly summarize key differences in these alternative radar systems that informed our selection for radar instrumentation. The VISAR radar system that will fly on NASA's VERITAS mission is designed for interferometry, which would not be necessary or conducive to meeting the science objectives of this mission concept. The mission design proposed for THUNDER is also fundamentally different from that for VERITAS, in large part driven by the distance to target body, radar power requirements, and power subsystem capabilities and data transmission rates for a spacecraft in the outer vs. inner solar system. While the radar system described by Mastrogiuseppe 2019 is specific to a Titan orbiter, this radar system is also likely not feasible for the constraints and guidelines of this specific study, which were set by the Planetary Science Summer School and the New Frontiers 5 draft AO. The Mastrogiuseppe 2019 radar requires an antenna that is double in size (4-m vs. THUNDER's 2-m antenna) and mass (40 kg vs. THUNDER's 20 kg radar mass), so selecting this system would translate to increased wet and dry masses, increased instrument costing, and a lower delta-v budget for the mission. The cited heritage for the Mastrogiuseppe radar system is Cassini RADAR, which was originally considered as an option for THUNDER's radar instrumentation, but ultimately could not be accommodated due to mass and cost limitations. Additionally, the Cassini RADAR high-gain antenna was developed and contributed by the Italian Space Agency (ASI), and under the PSSS guidelines, we were not able to consider foreign agency contributions in our mission concept. Including a more "advanced" radar system is trade that could be considered by New Frontiers mission concept teams, but it may come at the expense of reducing the scope of other instruments or removing them entirely to decrease payload mass and power, and/or a decrease to the in-flight delta-v budget, which may inhibit an orbiter mission. Alternatively, contributions from other space agencies may make this instrumentation affordable but would not solve the payload mass, power, and corresponding delta-v limitations.

6.2. *Concept of operations*

THUNDER's concept of operations (ConOps) schedule repeats over intervals of six orbits around Titan, a timespan similar in duration to 1 Earth day (Figure 8). This ConOps consists of four operational modes: (1) radar (SAR); (2) recharge; (3) radar (altimetry) + vis-IR spectrometer; and (4) gravity science/telecommunications (Figure 8). Passive radiometry can be done simultaneously with radar SAR and altimetry during modes 1 and 3. Radar SAR, altimetry, and communications can operate on the day and night sides of Titan, while the vis-IR spectrometer can only operate on the day side due to light constraints.

In one ConOps cycle, mode 1 operates on a 50% duty cycle followed by recharge (mode 2) for one orbit. Mode 3 operates on a 50% duty cycle followed by recharge (mode 2) for three orbits. Two consecutive orbits (an ∼8-hour window) are used for either gravity science or telecomms, which will alternate ConOps cycles at a cadence set by science needs. During cycles conducting gravity science, all science data are stored on the spacecraft until the subsequent telecomms window. THUNDER will maintain a circular, near-polar orbit (95-degree inclination) at 1,300 km altitude for the entirety of its science mission and will avoid eclipses at all points while in Titan orbit (see Section 7.1).

Because the vis-IR spectrometer and HGA (used for radar, gravity science, and telecomms) are both mounted nadir-pointing to the top of the spacecraft (see section 6.3), time is allotted for slewing the spacecraft between the four operational modes. HGA pointing directions for each operational mode are as follows: port or starboard with a viewing angle of 30°for radar SAR operation (mode 1); no pointing requirement for recharge (mode 2); nadir for radar altimetry and the vis-IR spectrometer (mode 3); and towards Earth for gravity science/telecomms (mode 4). The solar array design allows for orientation adjustments independent of the spacecraft pointing direction.

Table 2. Payload accommodation requirements imposed by instrumentation.

Payload Accommodation Requirements	Vis-IR Spectrometer	Radar SAR & Radiometry Mode	Radar Altimeter Mode	Gravity Science
CBE Mass (kg)	17.8 kg	20 kg		Included in telecoms
CBE Power (W) *Peak* *Average* *Standby*	Peak: 13.5 W Average: 8.8 W Standby 4 W	Peak: 169 W Average: 38 W Standby: 10 W	Peak: 34 W Average: 42 W Standby: 10 W	Included in telecoms
CBE Data Rate(s) (bps)	155 kbps post instrument processing 4:1 lossless compression	85 kbps + 1 kbps passive post instrument processing 2:1 lossless compression	24 kbps post instrument processing 2:1 lossless compression	Included in telecoms
Pointing *Knowledge (arcsec 1 σ)* *Control (arcsec 1 σ)* *Stability (arcsec / sec 1 σ)* *Slew (arcsec / sec)*	Pointing Knowledge: 206 arcsec 1 σ Control: 247 arcsec 1 σ Stability: 41 arcsec / sec 1 σ Slew: none	Pointing Knowledge: 10 arcsec 1 σ Control: 445 arcsec 1 σ Stability: 910 arcsec / sec 1 σ Slew: none	Pointing Knowledge: 24 arcsec 1 σ Control: 429 arcsec 1 σ Stability: 86 arcsec / sec 1 σ Slew: none	Pointing Knowledge: not applicable Control: 180 arcsec 1 σ Slew: none
Viewing Direction in Body Coordinates	Nadir	30° port or starboard	Nadir	Toward Earth
CBE Dimensions (LxWxH in m)	0.2 x 0.4 x 0.9 m	0.3 x 0.3 x 0.3 m 2.5 m HGA - shared with telecoms		Included in telecoms
CBE Cost ($M FY24)	$44M (FY24, CADRe documentation with margin)	$95.5M (FY24, NICM 10 parametric model) $12M HGA customization (FY24, NICM 10 parametric model)		Included in telecoms

THUNDER science objectives require 83% surface coverage with Radar SAR and altimetry (with 10% overlap in area between ground tracks) and 42% surface coverage (with 10% overlap in area between ground tracks) with the vis-IR spectrometer. Radiometry coverage will occur passively during SAR passes, covering the same locations on the globe. Geographic locations for required coverage are shown in Figures 9 and 10. The gravity science investigation requires ≥5 Earth months of orbit to resolve Titan's gravity field to spherical harmonic degree ≥15. Considering the spatial coverage requirements, corresponding data volumes (Figure 11), and the telecomms subsystem capabilities (described in Section 7.9), this ConOps requires a science mission duration of 3.6 years, and THUNDER is designed to maintain the required science orbit for ≥4.6 years.

Figure 8. THUNDER ConOps: Spacecraft pointing directions and day/night side measurement capabilities for operational modes 1-4 (top); example duty cycle for a 6-orbit ConOps cycle (bottom).

6.3. *Science summary and data sufficiency*

With the described schedule for operations, THUNDER will survey at least 83% of Titan's surface (Figure 9, Figure 10). This coverage will fully meet all mission requirements (Figure 11). The three objectives together will answer priority science questions about Titan's structure, liquids, and methane cycle, and in doing so address issues of planetary development and history that are applicable across the Solar System and beyond.

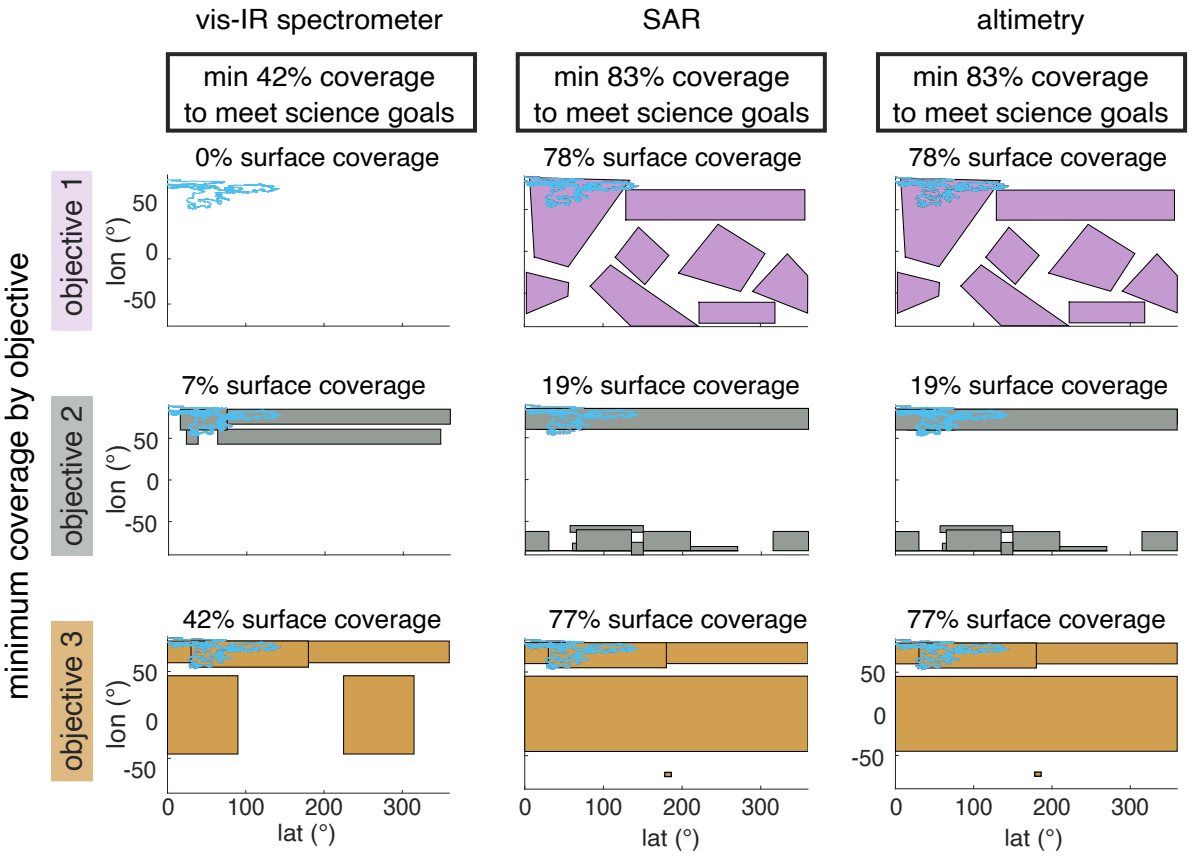

Figure 9. Coverage map for THUNDER's science goals, broken down by instrument, with column (a) showing vis-IR spectrometer, (b) for SAR coverage, and (c) for altimetry. The total amount of coverage by instrument is listed in the top row, enclosed by black boxes. All other rows correspond to each objective, with the minimum coverage needed per instrument per objective listed above polygons showing the map area required to meet science goals. The northern mare are outlined in the top right corner of each map, for orientation on Titan's surface

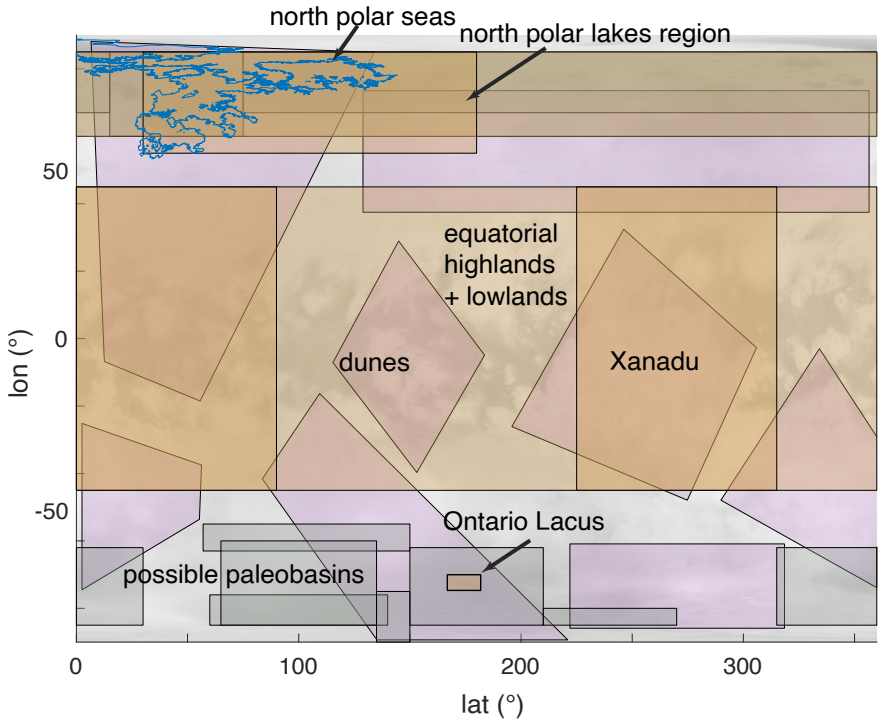

Figure 10. Total coverage map, overlaid on Cassini ISS imaging of Titan (credit NASA/JPL-Caltech/Univ. Arizona). Each objective corresponds to a specific colored polygon on the map, indicating total minimum coverage required for that objective across instruments. Several regions of interest are annotated on the map on the map. .

	Obj 1	Obj 2	Obj 3
Instruments/Modes	SAR / Altimetry / Gravity Science	SAR / Altimetry / Radiometry / Vis-IR	SAR / Altimetry / Radiometry / Vis-IR
Coverage	78% / 78% high-res,100% low-res/ 100% (global)	19% / 19% / 19% / 7% (polar)	77% / 77% / 42% / 42% (equatorial & polar)
Data Volume	320 Gbit / 14 Gbit / [telecom]	78 Gbit / 3.2 Gbit / 16 Mbit / 6 Gbit	320 Gbit / 13 Gbit / 16 Mbit / 18 Gbit
	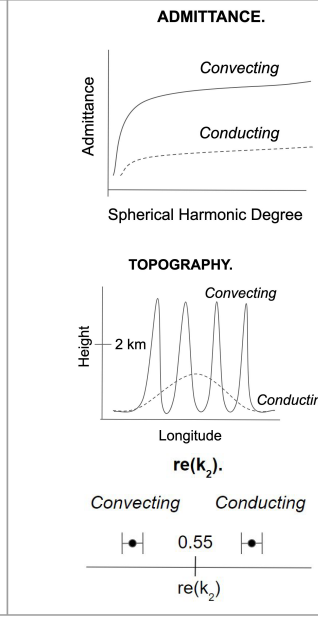	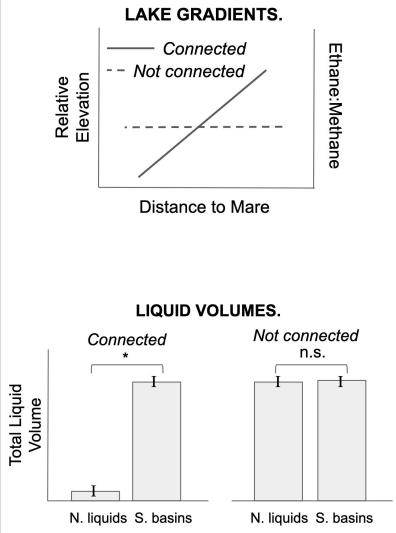	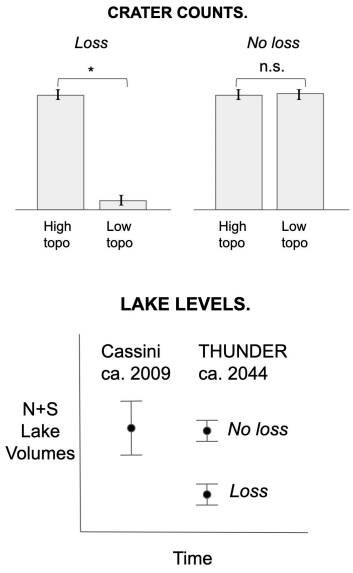

Figure 11. Data sufficiency by objective. Each objective, described above, will be fully answerable by THUNDER's proposed mission. This figure summarizes the necessary instrumentation, coverage, and data volume. Schematic figures of each physical parameter are shown in the bottom row, indicating end-member cases that can be differentiated using THUNDER's results.

7. MISSION DESIGN AND ENGINEERING

7.1. *Mission trajectory*

THUNDER's launch window will open on July 24, 2034 for a planned ten-year cruise to Saturn (Figure 12). An initial launch C_3 of 29.4 km^2/s^2 will be followed by an extended cruise phase with gravity assists from Venus, Earth, and Jupiter. This long cruise was chosen to minimize necessary Δv expenditure. Spacecraft operations and activity will be reduced during gaps between maneuvers longer than 12 months in duration. Radiation integrated dose from the Jovian space environment is expected to be minimal since the Jupiter Gravity Assist will take place at approximately $2.5x10^6$ km altitude, or 36 Jupiter radii, well outside of Jupiter's radiation belt.

Saturn Orbital Insertion (SOI) takes place on July 18, 2044. Mirroring Cassini, Thunder will achieve Saturn orbital insertion by flying through the E-F ring gap and then conduct a series of 10 Titan flybys over the course of 33 months to achieve Titan Orbital Insertion (TOI). This tour includes an unavoidable 2-hour solar eclipse soon after SOI, but our planned power reserves (Section 7.4) far exceed the amount needed to keep THUNDER operational through the loss of solar energy in this 2-hour period. At this point in mission design, possible flybys of other major Saturnian satellites and their incidental science potential have not been considered.

Following TOI, THUNDER will enter a 24 month pumpdown phase to the nominal science orbit. The science orbit will begin at 1,300 km altitude with an inclination of 95 degrees (Figure 13). The science orbit is formulated to minimize atmospheric drag, the risk of solar eclipses, and satisfy the surface illumination requirements of the Vis-IR instrument. As atmospheric drag on the spacecraft is a concern due to Titan's dense atmosphere and THUNDER's

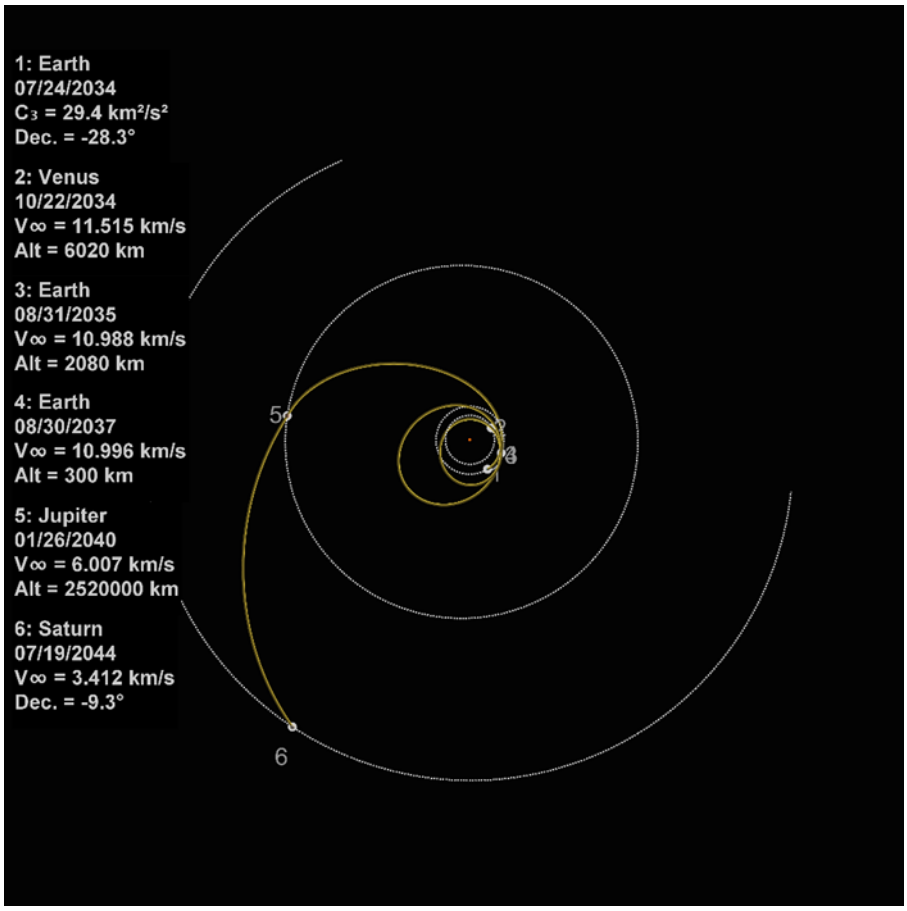

Figure 12. Planned THUNDER Cruise Phase trajectory from Launch to Saturn Orbital Insertion. Dates of flybys are listed, and planets are marked by numbers.

Figure 13. Diagram of nominal science orbit.

large solar arrays, we have chosen the 1,300 km science orbit altitude and will face the spacecraft at a 52.5°angle from head-on into its orbital path, which will decrease THUNDER's effective cross-sectional area by a factor of 0.6. This allows for a drag-makeup Δv budget of approximately 200 m/s to maintain the orbit over the duration of the mission, with 50 percent margin.

In order to avoid Titan solar eclipses, THUNDER must maintain an ascending node with a local time between 03:00 and 09:00 hours. At the same time, Vis-IR solar illumination requirements require ascending node placement between 08:00 and 16:00 local time. This provides a 1-hour window in which THUNDER may avoid solar eclipses while operating its Vis-IR instrument. THUNDER's placement in this one-hour orbital window is sustained by its 95 degree orbital inclination (Figure 13). This orbital inclination, while limiting our polar coverage, allows THUNDER's orbit to precess slowly relative to the sun, leading to a precession from an initial node of 09:00 to 08:00 over the course of 41 months, allowing us to satisfy our Vis-IR science requirements before the instrument is no longer able to function.

An additional 150 m/s Δv is budgeted for end-of-mission disposal of the spacecraft, which will allow for a targeted disposal on the surface of Titan. This disposal plan complies fully with NASA's planetary protection requirement, as the probability of contaminating liquid water by one viable terrestrial microorganism shall be less than 1 x 10^{-4} due to the short-lived nature of any possible melt pockets on the crust (Wakita et al. 2023) and our ability to avoid disposal in any regions that may appear to host liquid water.

7.2. *Configuration & launch services*

The THUNDER spacecraft design is informed by heritage spacecraft designs such as Juno, Europa Clipper, and Lucy. The base of the spacecraft bus includes the main engine (890N R-42DM, Aerojet), four thrusters (125N MR-107T, Aerojet), and the attitude determination and control system (ADCS) (Figure 14a). Power is generated using two UltraFlex solar arrays with a 9.5 m wing diameter. The wings are designed with two points of articulation to maintain a Sun-facing orientation throughout operation. The hexagonal bus design accommodates the oxidizer and bipropellant tanks used prior to Titan orbit insertion, conserves symmetry during fuel consumption, and allows these tanks to freeze off while in orbit to reduce thermal requirements during the science phase. The avionics are nested centrally with the monopropellant tank to conserve heat throughout operation. The radiator and star trackers are mounted on a side of the bus not shared by the solar array support hardware. The high-gain antenna (HGA), Vis-IR instrument, hold down and release mechanisms (HDRMs) for stabilizing the stowed solar arrays, Sun sensors, and telecom deck are mounted to the top of the spacecraft. Both instruments (the HGA and vis-IR spectrometer) are mounted in the nadir pointing direction. The bus was designed to avoid large custom tanks while maintaining compatibility with a 5-m payload fairing consistent with SpaceX's Falcon Heavy high performance launch vehicle (LV). Figure 14 also depicts THUNDER's stowed (c) and deployed (d) configurations.

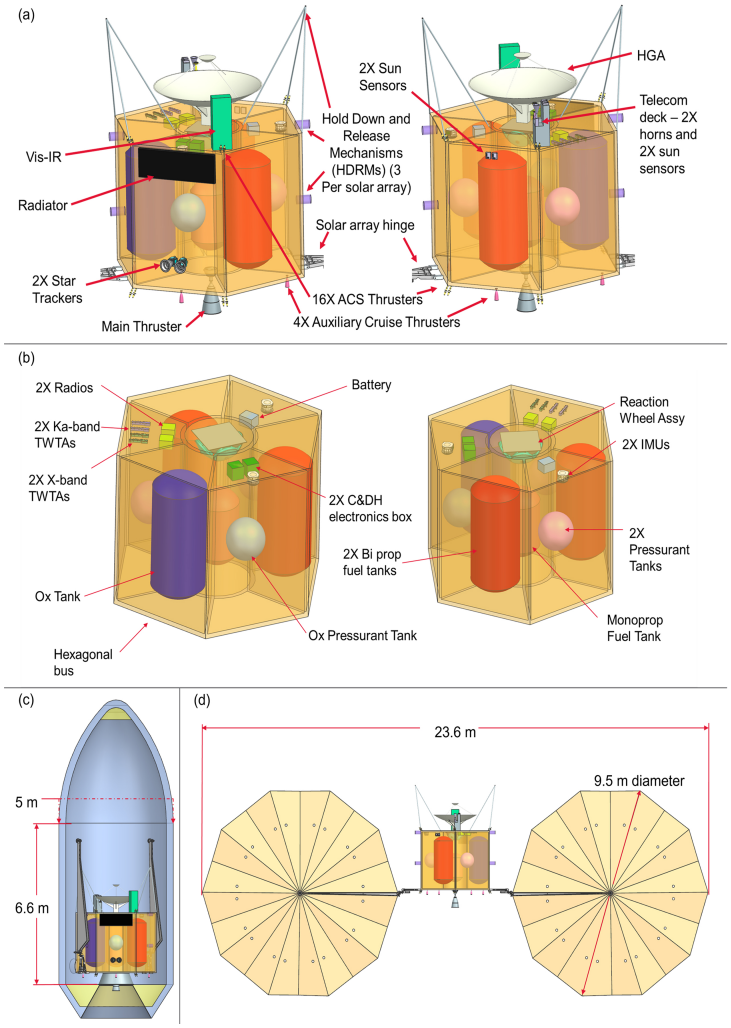

Figure 14. CAD models of THUNDER's external (a) and internal (b) components as well as THUNDER's stowed (c) and deployed (d) configurations.

The flight vehicle's total predicted wet mass is 5,053 kg, which includes the instrument payload, spacecraft system, propellant and pressurant. A high performance LV can carry a maximum of 5,880 kg (wet mass) for a launch C_3 of 29.4 km^2/s^2, resulting in a 16% margin for the flight vehicle wet mass. THUNDER's predicted dry mass (instrument

System	Predicted Mass (kg)	Margin	L/V Capability (kg)
Instrument Payload + Spacecraft System	1,690	47%	2,481
Propellant	3,363	1%	3,399
Flight Vehicle (Wet Mass)	**5,053**	**16%**	**5,880**

Table 3. THUNDER flight vehicle predicted wet mass, margin, and high performance launch vehicle capability. Spacecraft subsystem details are provided in Table 4.

Subsystem	Mass CBE (kg)	Contingency	Predicted Mass (kg)
Attitude Control	68.6	10%	75.4
Command & Data	8.3	17%	9.7
Power	233.8	29%	300.5
Telecomm	48.2	14%	54.8
Thermal	60.4	28%	77.3
Mechanical	581.1	30%	755.4
Propulsion: Hardware	269.3	3%	278.5
Propulsion: Residuals + Pressurant	91.5	0%	91.5
*Propulsion: Propellant**	*2,924*	*15%*	*3,363*
Spacecraft System (Dry Mass)	**1269.6**	**22%**	**1643.2**
Instrument Payload	**37.8**	**23%**	**46.5**

Table 4. Dry mass current best estimate (CBE), contingency, and predicted value for THUNDER instrument payload and each subsystem. *Propellant mass is not included in the spacecraft system (dry mass) total but is included here to show the planned contingency.

payload and spacecraft system) is 1,690 kg, which has a 47% margin for the high performance LV dry mass capability of 2,481 kg. Table 3 summarizes the flight vehicle predicted mass, LV capability, and mass margins. Instrument payload and subsystem mass current best estimates (CBEs), predicted mass, and contingencies are provided in Table 4.

7.3. *Propulsion*

THUNDER's propulsion system has one dual mode bi-propellant main engine utilizing hydrazine as its fuel and nitrogen tetroxide (NTO) as its oxidizer, which provides enough thrust for high Delta-V maneuvers during the tour, including a one-hour burn to initiate Titan orbit insertion. Four mono-propellant secondary thrusters use hydrazine as their fuel and provide thrust for moderate Delta-V maneuvers during the tour, drag corrections during Titan orbit, and end-of-mission disposal. Two sets of mono-propellant Reaction Control System (RCS) thrusters (one redundant) are used for ADCS wheel desaturation during Titan orbit. The fuel system is segmented such that all maneuvers during Titan orbit are performed using the monopropellant engines with a single isolated auxiliary tank of hydrazine fuel to save on heating power. The propellant system is sized to the maximum launch vehicle (LV) allocation, which provides a 15% fuel mass contingency for possible launch mass growth.

7.4. *Power*

THUNDER will be equipped with two flexible and deployable wings of UltraFlex solar arrays. The solar array is sized for a Saturn operating environment with a total area of 129 m^2, solar cell area of 109 m^2, and wing diameter of 9.5 m. The solar array will be integrated with inverted metamorphic multijunction (IMM) solar cells due to their low mass, ultra-high efficiency, and flexibility. The IMM solar cells will have a 30% efficiency at air mass zero, 1 AU, and 20°C, although solar cell efficiency decreases with increasing distance from the sun and solar cell life. The expected power generation of the solar array for the THUNDER mission at the beginning of life will be 4,800 W, decreasing towards 440 W at the end of life. During THUNDER's science tour in Titan orbit, it is expected that the solar array will be able to generate ∼496 W. Generated power will be stored in a Lithium-ion battery with 9 cells and a 36 Ah storage capacity, which has the capability to store 1,050 Wh of energy. The battery was sized for the unavoidable 2-hour solar eclipse in the mission design after SOI, which is the only time during the mission that THUNDER will

	LD	SPO	SW	BTB	SVA	SS	COy	EQ	R	CHD
Mode duration (h)	2	24	24	1	2	2	9	2	2	2
Sub of Subsystems' Power (W)	270	495	508	549	357	530	411	271	292	338
Required Energy for Subsystems (Wh)	538	11894	12185	550	786	1166	3617	543	643	744
Array Capability (Wh)	0	11894	11894	496	1090	1090	4361	0	1090	1090
Battery Discharge Energy (Wh)	-538	0	-291	-54	305	-75	744	-543	448	347
Battery Capability (Wh)	1166	1050	1050	1050	1050	1050	1050	1050	1050	1050

Table 5. THUNDER's power requirements and capability for operational modes and key spacecraft maneuvers: Launch + Deploy (LD), Safe mode - Propulsion only (SPO), Safe mode - Wheels (SW), Bipropellant Titan Orbital Insertion Burn (BTB), Science mode - VisIR + Atimeter (SVA), Science mode - SAR (SS), Communications only (CO), Eclipse mode - Quiescent (EQ), Recharge (R), and Catbed heating and desat (CHD).

be completely in the dark. The worst-case battery depth of discharge (DOD) will be 50% over the mission lifetime, providing substantial margin for the power subsystem. Further, the space bus voltage is 32 V, which is informed by the maximum power requirement and selected to minimize both generated current through the spacecraft and mass of the voltage system.

The power subsystem was designed based on the highest energy operational mode, which is THUNDER's $\leq$ 24-hour safe mode (using reaction wheel actuators). The safe mode power requirement is 508 W, which includes a 43% contingency, when all non-essential systems are shut down. If the spacecraft is in safe mode for 24 hours, 12,185 Wh of energy are required to maintain essential systems: attitude control, propulsion, telecomm, thermal, and power. The solar array capability during safe mode is 11,894 Wh (496 W for 24 hours), and the battery provides the remaining energy requirement of 291 Wh ($\sim$28% DOD). THUNDER's power requirements and power capability for each operational mode are listed in Table 5.

7.5. *Thermal Control*

With a cruise trajectory perihelion of 0.61 AU and target destination at 9.5 AU, THUNDER requires additional thermal precautions to function at both near-solar and outer solar system temperature conditions. The thermal design for the spacecraft is primarily informed by the worst-case cold (WCC) and worst-case hot (WCH) thermal scenarios during the full mission trajectory (see section 7). THUNDER's cruise includes a flyby of Venus at 0.7 AU, which is the WCH scenario with an expected solar flux of 2,700 W/m^2. Safe-mode at Saturn pre-TOI is the WCC scenario with an expected solar flux of 15 W/m^2. To operate across the expected temperature range, THUNDER uses a heating system with loop heat pipes and a switch that allows the spacecraft to actively dump heat during the WCH and to passively direct heat into the propellant tanks during the WCC. The thermal subsystem includes six loop heat pipes: one for each avionics unit plus one redundant set. The design also includes standard multi-layer insulation (MLI) blankets with 97% insulation effectiveness.

7.5.1. *Worst-case hot (WCH) scenario: Venus flyby*

During the Venus flyby, the heat pipe system will be a closed loop so that heat from the propellant tanks will be actively redirected to the radiators. The radiators' combined surface area is 1.38 m^2 and is sized based on the WCH thermal conditions with the following assumptions: distance from Venus is great enough so that IR loads are negligible; and a flight rule is imposed so that the radiators are not in view of the Sun. In addition to positioning the radiators so that they are not in view of the Sun during the Venus flyby, the HGA will be pointed at the Sun to shield as much of the spacecraft as possible. These flight rules may be necessary at distances up to 5 AU, but further analysis and design are required to refine this range. THUNDER will operate in a comms-only mode during the Venus flyby to reduce heat production associated with instrument operations. With these flight rules and closed-loop heat pipe system, the propulsion bay (partially exposed to the Sun) and the HGA (directly exposed to the Sun) do not exceed their temperature limits during the WCH scenario.

7.5.2. *Worst-case cold (WCC): Saturn orbit, pre-TOI*

Once THUNDER is >5 AU (further analysis is required to refine this distance), the heat pipe system will switch from directing heat away from the propellant tanks to allowing the avionics to passively radiate onto the tanks. After TOI, only one auxiliary fuel tank is needed to maintain the Titan orbit and end of mission disposal requirements, so the main engine (biprop) fuel and oxidizer tanks will be thermally sequestered and allowed to freeze. This reduces the heater power requirement from 206 W to 34 W during the science tour at Titan. Radioisotope heating units (RHUs) are not required because the avionics dissipate sufficient heat into the bus, and they are nested between propulsion tanks to maintain the required temperature pre- and post-TOI.

7.6. *Attitude determination and control*

Scientific objective (Sections 2-4) and instrumentation requirements for the THUNDER mission drive the requirements for the attitude determination and control system (ADCS). The minimum knowledge, control, and stability errors in Table 2 are the pointing requirements for the spacecraft. The spacecraft is three-axis stabilized with dual-redundancy for sensors and 4:3 redundancy for reaction wheel actuators (RWAs). The onboard sensors for attitude determination will include 4 Adcole two-axis digital sun sensors, 2 SSTL Procyon star trackers, and 2 Honeywell YG99666Hz miniature inertial measurement units (MIMUs). The spacecraft will use 4 Honeywell HR16 RWAs and 2 MOOG 2-channel electronic control units (ECUs) for attitude control. All sensors and actuators used for attitude determination and control are at Technology Readiness Level (TRL) 9.

The actuators are capable of obtaining ≥10 arcsec knowledge error, matching the 10 arcsec error requirement set by radar SAR (Table 2). The ADCS subsystem control and stability/jitter capabilities will be determined during Phase B and C respectively, and are expected to meet the requirements listed in Table 2 with adequate margin.

To mitigate propellant depletion of the Reaction Control System (RCS) thrusters during the cruise phase, the RWAs will be used to point the HGA and solar arrays for communication and power, respectively. The use of the RCS as backup will serve as a contingency in the event of a RWA failure throughout Phase E.

7.7. *Flight software*

We use the F Prime software package for base framework as it is compatible with and optimized for our selected flight hardware package (see section 7.8). Of the estimated one million lines of code, we can reuse approximately 55% of the total lines of code from previous missions. Most of the new code development occurs at the application level where mission specific tasks are performed (e.g., special flight maneuvers, solar panel deployment, etc.). A spiral development method is used for testing and implementation of all new and modified software; this method allows for an iterative approach and therefore optimizes risk management throughout development. Most software development is scheduled during Phases C and D, and software updates will be performed remotely during cruise as needed.

7.8. *Command and data handling*

THUNDER will use a Sphinx flight computer, adequate to meet the mass and volume constraints of the mission. The Sphinx has a 10 cm by 10 cm footprint and weighs 250 grams. The Sphinx was flown in NASA's Artemis I and Lunar Flashlight missions, and so has the heritage to meet the New Frontiers mission requirement of technology readiness level (TRL) ≥ 6. The flight computer will compress and store the raw science and housekeeping data. Since Sphinx can store up to 64 Gbits, and THUNDER will produce 340 Mbit/day of science data and 86.4 Mbit/day of housekeeping data, we can store up to 100 days of generated data. This storage capability will protect THUNDER from any missed passes and allow for dedicated gravity science orbits. Although THUNDER's data downlink will consist of a daily 8-hour pass, given THUNDER's data transmission rate of 12 kbps, we only need 6.12 hours to transmit the compressed data collected over one ConOps cycle. Additional downlink time (up to 8 hours) will be required after cycles where gravity science is conducted in place of telecomms.

7.9. *Telecommunications and ground systems*

The telecommunications subsystem is designed with a 2-meter high gain antenna capable of X-band uplink and downlink and Ka-band uplink and downlink. Nominal uplink will occur at 2 kbps and nominal downlink at 12 kbps. All data rates are achieved with greater than 3 dB margin to 34-meter DSN stations. Additional capabilities with regards to Ka-band are needed to achieve gravity science-based objectives. While not currently common for deep space missions, use of the Ka-band communications system can aid in relief of long-term scheduling stress on NASA's

Deep Space Network, as requested in the New Frontiers 5 Draft Announcement of Opportunity. A traditional X-band system is included for the dual-purpose HGA radar requirements and also serves as a fully redundant backup telecomms system, since Ka-band communications, over a very thin beamwidth, have not yet been demonstrated from the outer Solar System distances required for this mission.

Nominal data downlink is baselined to occur via a single 8-hour pass on a DSN 34-meter antenna per day, as required by the New Frontiers 5 Draft Announcement of Opportunity. However, critical spacecraft maneuvers, such as Saturn orbit insertion, are allowed to utilize temporarily increased DSN coverage, such as multiple 34-meter antennas and/or a 70-meter antenna. Radio science investigations, navigation observations (e.g., delta differential one-way ranging), and spacecraft emergencies are exempt from these restrictions, but will still need to be negotiated with DSN scheduling as needed throughout the mission.

8. RISKS

The risks inherent to this mission are associated primarily with the long duration of the mission and the development of the solar array and radar technology. Reserves in cost and schedule should be allocated for universal risks like supply chain delays or delays in the AO/Step-2 release. Delays in the funding and selection schedules can also affect the launch window, which may require changing the mission trajectory and associated subsystem requirements. For the mission design presented here, the arrival is after Titan summer solstice, which is suitable to meet mission goals, and delays further into autumn would only improve the comparison with past missions.

The UltraFlex solar array technology has been developed and demonstrated up to a high ($\geq$6) TRL but at a smaller size (7.3-m diameter for NASA's Lucy mission) than the one required for mission design. Larger UltraFlex technology called MegaFlex (with 9.6-m diameter) has been flown in-atmosphere (TRL 5), but has not yet completed a space flight demonstration. To mitigate this issue, the following actions were implemented: 1) including cost reserves for testing and development of the increased size, 2) beginning the development in Phase A, 3) preparing to employ the high-heritage and high-TRL ROSA technology if the UltraFlex technology is deemed not feasible following a review decision at the preliminary design review (PDR; following phase B). While the ROSA technology can be used if necessary, the UltraFlex solar arrays are preferred for this mission because of their lower mass and smaller stowed volume in comparison.

THUNDER requires a Radar/SAR. The technology the mission will use is at TRL $\geq$6 with a different configuration. The specific design of the radar SAR/Altimeter that THUNDER will use is based on the D2P instrument, which was developed under an IIP and has been flown in atmosphere (Mitri et al. 2018). Here again, mitigation is provided by including cost and schedule reserves, with the engineering model build before PDR to ensure the selected radar instrument meets TRL requirements.

The long time scale of this mission increases the risk of 1) component degradation, 2) test-bed degradation, and 3) loss of experience in the workforce. For the first two of those items involving degradation of equipment, it is recommended to use accelerated life testing of vital components (e.g. RWA) and that the RCS thruster be used as backup while in Saturn/Titan orbit. For the third item concerning personnel, THUNDER plans for 2.0 (shared) FTE over the cruise phase including preparatory activities and outreach, as well as an emphasis on documentation, and the deputy PI's involvement from conception.

9. COST

The total PI-managed mission cost for THUNDER is \$1,518.2M in Fiscal Year (FY) 2024, divided into \$1,126.5M for Phases A-D, including Launch Vehicle, and \$391.7M for Phases E-F. This considers a Class-B mission, and in-house development and operations at JPL. Table 6 presents the cost breakdown per mission phase, and Table 7 the cost per Work Breakdown Structure (WBS).

The mission considered a cost cap of \$1,650M FY 2024 for the PI-managed mission cost, divided into \$1,240M for Phases A-D (development cost) and \$410M for Phases E-F (operations cost). As per the draft NF 5 AO, 25% reserves are required for Phases A-D, as well as 25% for Phases E-F, Phase A cost is set at \$5M, and the High-Performance Launch Vehicle with a 5 m fairing required for the mission adds \$77M towards the development cost. Education and Public Outreach are accounted for in the total mission cost, not the PI-managed cost, therefore are set to 0.

JPL's Institutional Cost Model (ICM) was used to estimate mission costs, relying on parametric modeling and analogies from previous missions. NASA's ICM payload cost model was used for the radar cost, while the Vis-IR instrument cost was based on the cost of development completion for OSIRIS-REx's OVIRS instrument. Mitigation

Table 6. PI-managed cost estimates A-F (FY24)

	Cost without reserves	Cost with reserves
TOTAL	**$1199.6 M**	**$1518.2 M**
Phase A	$5.0 M	$5.0 M
Phase B	$82.2 M	$106.8 M
Phases C/D	$721.4 M	$937.7 M
Launch Vehicle	$77.0 M	$77.0 M
Phases E/F	$314.0 M	$391.7 M

costs were pre-allocated to the main mission risks, including additional testing and development of the UltraFlex solar arrays and the radar instrument. These mitigation costs do not include the 30% reserves included for Phases A-D, exceeding the AO requirement by 5%, and 25 % for Phases E-F, as per the AO. An initial cost validation was performed per WBS using past New Frontiers mission data. Cost estimates for THUNDER per WBS are within +/− 13% of the average WBS cost for past accepted New Frontiers mission costs. Future validation would include estimating the mission's cost with other industry models.

Table 7. Cost by Work Breakdown Structure (WBS) with reserves

WBS Cost Breakdown		Development Cost (Phases B-D)	Operations Cost (Phases E-F)
Total Cost		**$1121.5 M**	**$391.7 M**
01.0	Project Management	$17.6 M	$24.6 M
02.0	Project Systems Engineering	$33.6 M	$1.1 M
03.0	Mission Assurance	$37.4 M	$5.6 M
04.0	Science	$14.9 M	$55.6 M
05.0	Payload System	$154.8 M	$0.0 M
06.0	Flight System	$415.9 M	$0.0 M
07.0	Mission Operations Preparation	$31.4 M	$199.2 M
08.0	Launch Vehicle	$77.0 M	$0.0 M
09.0	Ground Data Systems	$22.9 M	$27.9 M
10.0	ATLO	$52.7 M	$0.0 M
11.0	Education and Public Outreach	$0.0 M	$0.0 M
12.0	Mission and Navigation Design	$22.4 M	$0.0 M
	Reserves	$240.9 M	$77.7 M

10. ENVIRONMENTAL IMPACTS

Anthropogenic climate change is severely threatening the cultural and physical health of communities around the globe, as well as driving habitat loss and general extinction of many species (Intergovernmental Panel On Climate Change 2023). In line with NASA's Climate Strategy and the societal responsibility inherent to taxpayer-funded mission design, the THUNDER mission will therefore minimize its climate impacts to the greatest extent possible at every stage of planning and design. This will involve emphasis on virtual meetings during Phases A-B of the mission (while remaining mindful of accessibility concerns), commitment to conducting climate studies in both the planning and building phases of all subsystems related to the mission, and direct quantification of the cumulative greenhouse gas emissions related to the mission (including and exceeding those related to propellant burn necessary for launch), following methods similar to financial auditing. Similar methods have been used to assess the carbon impacts resulting from the InSight mission (Bill et al. 2023), and proposed for the upcoming Flagship mission to the Uranian system (Fernando et al. 2024). Public outreach and education will also emphasize the importance of responsible climate practices in mission planning, reminding the public that NASA science is for everyone. In building THUNDER with sustainability in mind from the beginning, we thus hope to serve as a positive example for future missions.

11. CONCLUSION

The THUNDER mission's science objectives fully characterize Titan as an active, dynamic world of its own. Using vis-IR spectrometry, three radar modes, and gravity science, this mission investigates how the evolution and present-day appearance of Titan's surface reflects its unique hydrocarbon cycle, and what this implies for the moon's habitability through time. In doing so, this mission will revolutionize our understanding not only of Titan, but of fluvially modified worlds, past and present, across the Solar System, as well as of other icy moons in comparison. We will discover the thermal characteristics of Titan's ice shell, track subsurface material transport, and determine the relative age of Titan's hydrocarbon-rich atmosphere and surface liquids. Our geological and geophysical measurements will complement the small-scale atmospheric and subsurface properties that the Dragonfly mission will observe, encouraging Titan science well into the future. However, the mission concept is incomplete, and will benefit from future study at all levels. A future version of the THUNDER mission could provide better insight into relative dating of Titan's crust, effects and extent of clathratization on the icy shell, and mechanisms and timescales of erosion.

12. ACKNOWLEDGEMENTS

Thanks to PSSS Administrator Joyce Armijo, PSSS School Manager Leslie Lowes, JPL's Team X, JPL, NASA, and the proposal reviewers. The authors would also like to acknowledge Bruce Campbell, Mike Malaska, Bill Smthye, Sarah Hörst, Jason Soderblom, Ryan Park, and Brian Sutin for their helpful discussions. We would also like to thank two anonymous reviewers for their thoughtful, constructive commentary on the science and design aspects of this paper, as well as PSJ editorial staff for their careful handling and discussion of the content and framing. The cost information contained in this document is of a budgetary and planning nature and is intended for informational purposes only. It does not constitute a commitment on the part of JPL and/or Caltech. The information provided is pre-decisional and for planning and discussion purposes only. The research was carried out at the Jet Propulsion Laboratory, California Institute of Technology, under a contract with the National Aeronautics and Space Administration (80NM0018D0004).

REFERENCES

2023, Origins, Worlds, and Life: A Decadal Strategy for Planetary Science and Astrobiology 2023-2032 (Washington, D.C.: National Academies Press), doi: 10.17226/26522

Aharonson, O., Hayes, A. G., Lunine, J. I., et al. 2009, Nature Geoscience, 2, 851, doi: 10.1038/ngeo698

Akiba, R., Ermakov, A. I., & Militzer, B. 2022, The Planetary Science Journal, 3, 53, doi: 10.3847/PSJ/ac4d2b

Applied Physics Laboratory, J. H. U. 2008. https://www.lpi.usra.edu/opag/Titan_Explorer_Public_Report.pdf

Barnes, J. W., Buratti, B. J., Turtle, E. P., et al. 2013, Planetary Science, 2, 1, doi: 10.1186/2191-2521-2-1

Barth, E. L., & Toon, O. B. 2006, 182, 230, doi: 10.1016/j.icarus.2005.12.017

Beuthe, M. 2021, Geophysical Journal International, 227, 693, doi: 10.1093/gji/ggab241

Biersteker, J. B., Weiss, B. P., Cochrane, C. J., et al. 2023, The Planetary Science Journal, 4, 62, doi: 10.3847/PSJ/acc331

Bill, C. A., Fernando, B. A., Schmerr, N., & Banerdt, W. B. 2023, There is No Planet B: An Initial Assessment Framework to Calculate the Environmental Impact of the InSight Mars Mission. https://www.hou.usra.edu/meetings/lpsc2023/pdf/1742.pdf

Birch, S., Hayes, A., Corlies, P., et al. 2018, Icarus, 310, 140, doi: 10.1016/j.icarus.2017.12.016

Birch, S. P. D., Hayes, A. G., Dietrich, W. E., et al. 2017, Icarus, 282, 214, doi: 10.1016/j.icarus.2016.08.003

Blanc, M., Prieto-Ballesteros, O., André, N., et al. 2020, Planetary and Space Science, 193, 104960, doi: 10.1016/j.pss.2020.104960

Brown, M. E., Schaller, E. L., Roe, H. G., et al. 2009, Geophysical Research Letters, 36, doi: https://doi.org/10.1029/2008GL035964

Brown, R. H., Soderblom, L. A., Soderblom, J. M., et al. 2008, Nature, 454, 607, doi: 10.1038/nature07100

Burr, D. M., Drummond, S. A., Cartwright, R., Black, B. A., & Perron, J. T. 2013a, Icarus, 226, 742, doi: 10.1016/j.icarus.2013.06.016

Burr, D. M., Taylor Perron, J., Lamb, M. P., et al. 2013b, GSA Bulletin, 125, 299, doi: 10.1130/B30612.1

Carnahan, E., Vance, S. D., Hesse, M. A., Journaux, B., & Sotin, C. 2022, Geophysical Research Letters, 49, e2021GL097602, doi: 10.1029/2021GL097602

Cassini magnetometer team. 2017, Astronomy & Geophysics, 58, 4.36, doi: 10.1093/astrogeo/atx140

Choukroun, M., Grasset, O., Tobie, G., & Sotin, C. 2010, Icarus, 205, 581, doi: 10.1016/j.icarus.2009.08.011

Choukroun, M., & Sotin, C. 2012, Geophysical Research Letters, 39, doi: 10.1029/2011GL050747

Cook-Hallett, C., Barnes, J. W., Kattenhorn, S. A., et al. 2015, Journal of Geophysical Research: Planets, 120, 1220, doi: 10.1002/2014JE004645

Cordier, D., Mousis, O., Lunine, J. I., et al. 2012, Planetary and Space Science, 61, 99, doi: 10.1016/j.pss.2011.05.009

Corlies, P., Hayes, A. G., Birch, S. P. D., et al. 2017, Geophysical Research Letters, 44, 11,754, doi: 10.1002/2017GL075518

Corlies, P., McDonald, G. D., Hayes, A. G., et al. 2021, Icarus, 357, 114228, doi: 10.1016/j.icarus.2020.114228

Cottini, V., Nixon, C. A., Jennings, D. E., et al. 2012, 60, 62, doi: 10.1016/j.pss.2011.03.015

Dhingra, R. D., Barnes, J. W., Brown, R. H., et al. 2019, Geophysical Research Letters, 46, 1205, doi: 10.1029/2018GL080943

Dhingra, R. D., Barnes, J. W., Heslar, M. F., et al. 2020, The Planetary Science Journal, 1, 31, doi: 10.3847/PSJ/ab9c2b

Durante, D., Hemingway, D. J., Racioppa, P., Iess, L., & Stevenson, D. J. 2019, Icarus, 326, 123, doi: 10.1016/j.icarus.2019.03.003

Elachi, C., Wall, S., Allison, M., et al. 2005, Science, 308, 970, doi: 10.1126/science.1109919

Ermakov, A. I., Fu, R. R., Castillo-Rogez, J. C., et al. 2017, Journal of Geophysical Research: Planets, 122, 2267, doi: 10.1002/2017JE005302

Faulk, S. P., Lora, J. M., Mitchell, J. L., & Milly, P. C. D. 2020, Nature Astronomy, 4, 390, doi: 10.1038/s41550-019-0963-0

Fernando, B., Pontrefract, A., Seltzer, C., et al. 2024, Environmental Impact Considerations for the Uranus Orbiter Probe Mission

Genova, A., Goossens, S., Lemoine, F. G., et al. 2016, Icarus, 272, 228, doi: 10.1016/j.icarus.2016.02.050

Goossens, S., van Noort, B., Mateo, A., Mazarico, E., & van der Wal, W. 2024, Nature Astronomy, 8, 846, doi: 10.1038/s41550-024-02253-4

Graves, S. D. B., McKay, C. P., Griffith, C. A., Ferri, F., & Fulchignoni, M. 2008, Planetary and Space Science, 56, 346, doi: 10.1016/j.pss.2007.11.001

Griffith, C. A., Penteado, P., Rannou, P., et al. 2006, Science, 313, 1620, doi: 10.1126/science.1128245

Hayes, A., Aharonson, O., Callahan, P., et al. 2008, Geophysical Research Letters, 35, doi: 10.1029/2008GL033409

Hayes, A. G. 2016, Annual Review of Earth and Planetary Sciences, 44, 57, doi: 10.1146/annurev-earth-060115-012247

Hayes, A. G., Aharonson, O., Lunine, J. I., et al. 2011, Icarus, 211, 655, doi: 10.1016/j.icarus.2010.08.017

Hayes, A. G., Birch, S. P. D., Dietrich, W. E., et al. 2017, Geophysical Research Letters, 44, 11,745, doi: 10.1002/2017GL075468

He, C., & Smith, M. A. 2014, Icarus, 238, 86, doi: 10.1016/j.icarus.2014.05.012

Hedgepeth, J. E., Neish, C. D., Turtle, E. P., et al. 2020, Icarus, 344, 113664, doi: 10.1016/j.icarus.2020.113664

Hemingway, D., Nimmo, F., Zebker, H., & Iess, L. 2013, Nature, 500, 550, doi: 10.1038/nature12400

Hensley, S., Campbell, B., Perkovic-Martin, D., et al. 2020, in 2020 IEEE Radar Conference (RadarConf20), 1–6, doi: 10.1109/RadarConf2043947.2020.9266323

Horvath, D. G., Andrews-Hanna, J. C., Newman, C. E., Mitchell, K. L., & Stiles, B. W. 2016, Icarus, 277, 103, doi: 10.1016/j.icarus.2016.04.042

Hörst, S., Yelle, R., Buch, A., et al. 2012, Astrobiology, 12, 809, doi: 10.1089/ast.2011.0623

Hörst, S. M. 2017, Journal of Geophysical Research: Planets, 122, 432, doi: 10.1002/2016JE005240

Iess, L., Jacobson, R. A., Ducci, M., et al. 2012, Science, 337, 457, doi: 10.1126/science.1219631

Intergovernmental Panel On Climate Change. 2023, Climate Change 2022 – Impacts, Adaptation and Vulnerability: Working Group II Contribution to the Sixth Assessment Report of the Intergovernmental Panel on Climate Change, 1st edn. (Cambridge University Press), doi: 10.1017/9781009325844

Janssen, M., Lorenz, R., West, R., et al. 2009, Icarus, 200, 222, doi: https://doi.org/10.1016/j.icarus.2008.10.017

Janssen, M., Le Gall, A., Lopes, R., et al. 2016, Icarus, 270, 443, doi: https://doi.org/10.1016/j.icarus.2015.09.027

Jennings, D. E., Cottini, V., Nixon, C. A., et al. 2011, 737, L15, doi: 10.1088/2041-8205/737/1/L15

Kalousová, K., & Sotin, C. 2020a, Earth and Planetary Science Letters, 545, 116416, doi: 10.1016/j.epsl.2020.116416

—. 2020b, Geophysical Research Letters, 47, e2020GL087481, doi: 10.1029/2020GL087481

Konopliv, A. S., Asmar, S. W., Folkner, W. M., et al. 2011, Icarus, 211, 401, doi: 10.1016/j.icarus.2010.10.004

Larsson, R., & McKay, C. P. 2013, Planetary and Space Science, 78, 22, doi: 10.1016/j.pss.2012.12.001

Le Gall, A., Malaska, M. J., Lorenz, R. D., et al. 2016, Journal of Geophysical Research: Planets, 121, 233, doi: 10.1002/2015JE004920

Le Mouélic, S., Cornet, T., Rodriguez, S., et al. 2019, Icarus, 319, 121, doi: 10.1016/j.icarus.2018.09.017

Lefevre, A., Tobie, G., Choblet, G., & Čadek, O. 2014, Icarus, 237, 16, doi: 10.1016/j.icarus.2014.04.006

Liu, Z. Y.-C., Radebaugh, J., Harris, R. A., et al. 2016, Icarus, 270, 14, doi: 10.1016/j.icarus.2015.11.021

Lopes, R. M. C., Malaska, M. J., Schoenfeld, A. M., et al. 2019a, Nature Astronomy, 4, 228, doi: 10.1038/s41550-019-0917-6

Lopes, R. M. C., Wall, S. D., Elachi, C., et al. 2019b, Space Science Reviews, 215, 33, doi: 10.1007/s11214-019-0598-6

Lora, J. M., & Mitchell, J. L. 2015, Geophysical Research Letters, 42, 6213, doi: 10.1002/2015GL064912

Lorenz, R. D. 2000, Science, 290, 467, doi: 10.1126/science.290.5491.467

—. 2014a, Meteoritics & Planetary Science, 49, 1139, doi: 10.1111/maps.12317

—. 2014b, Geophysical Research Letters, 41, 5764, doi: 10.1002/2014GL061133

—. 2021, Journal of Geophysical Research: Planets, 126, e2020JE006786, doi: 10.1029/2020JE006786

Lorenz, R. D., Leary, J. C., Lockwood, M. K., Waite, J. H., & El-Genk, M. S. 2008, in AIP Conference Proceedings, Vol. 969 (Albuquerque (New Mexico): AIP), 380–387, doi: 10.1063/1.2844991

Lorenz, R. D., Niemann, H. B., Harpold, D. N., Way, S. H., & Zarnecki, J. C. 2006, Meteoritics & Planetary Science, 41, 1705, doi: 10.1111/j.1945-5100.2006.tb00446.x

Lorenz, R. D., Kirk, R. L., Hayes, A. G., et al. 2014, 237, 9, doi: 10.1016/j.icarus.2014.04.005

Lunine, J. I., & Atreya, S. K. 2008, Nature Geoscience, 1, 159, doi: 10.1038/ngeo125

Lunine, J. I., Cable, M. L., Horst, S. M., & Rahm, M. 2020, The Astrobiology of Titan, doi: 10.2458/azu_uapress_9780816540068

MacKenzie, S. M., Barnes, J. W., Sotin, C., et al. 2014, Icarus, 243, 191, doi: 10.1016/j.icarus.2014.08.022

MacKenzie, S. M., Birch, S. P. D., Hörst, S., et al. 2021, The Planetary Science Journal, 2, 112, doi: 10.3847/PSJ/abf7c9

Malaska, M. J., Hodyss, R., Lunine, J. I., et al. 2017, Icarus, 289, 94, doi: https://doi.org/10.1016/j.icarus.2017.01.033

Marusiak, A. G., Panning, M. P., Vance, S. D., et al. 2022, Earth and Space Science, 9, e2021EA002041, doi: 10.1029/2021EA002041

Mastrogiuseppe, M. 2019, Remote Sensing, 11, 1898, doi: 10.3390/rs11161898

Mastrogiuseppe, M., Poggiali, V., Hayes, A. G., et al. 2019, Nature Astronomy, 3, 535, doi: 10.1038/s41550-019-0714-2

Mastrogiuseppe, M., Poggiali, V., Hayes, A., et al. 2014, Geophysical Research Letters, 41, 1432, doi: 10.1002/2013GL058618

Mastrogiuseppe, M., Hayes, A., Poggiali, V., et al. 2018, Icarus, 300, 203, doi: 10.1016/j.icarus.2017.09.009

Miller, J. W., Birch, S. P. D., Hayes, A. G., et al. 2021, The Planetary Science Journal, 2, 142, doi: 10.3847/PSJ/ac0245

Mitchell, K. L., Barmatz, M. B., Jamieson, C. S., Lorenz, R. D., & Lunine, J. I. 2015, Geophysical Research Letters, 42, 1340, doi: 10.1002/2014GL059475

Mitri, G., Bland, M. T., Showman, A. P., et al. 2010, Journal of Geophysical Research, 115, E10002, doi: 10.1029/2010JE003592

Mitri, G., Meriggiola, R., Hayes, A., et al. 2014, Icarus, 236, 169, doi: 10.1016/j.icarus.2014.03.018

Mitri, G., Postberg, F., Soderblom, J. M., et al. 2018, Planetary and Space Science, 155, 73, doi: 10.1016/j.pss.2017.11.001

Mousis, O., Choukroun, M., Lunine, J. I., & Sotin, C. 2014, Icarus, 239, 39, doi: 10.1016/j.icarus.2014.05.032

Mousis, O., Lunine, J. I., Hayes, A. G., & Hofgartner, J. D. 2016, Icarus, 270, 37, doi: https://doi.org/10.1016/j.icarus.2015.06.024

Neish, C., & Lorenz, R. 2014, Icarus, 228, 27, doi: 10.1016/j.icarus.2013.09.024

Neish, C. D., & Lorenz, R. D. 2012, Planetary and Space Science, 60, 26, doi: 10.1016/j.pss.2011.02.016

Neish, C. D., Molaro, J. L., Lora, J. M., et al. 2016, Icarus, 270, 114, doi: 10.1016/j.icarus.2015.07.022

Neish, C. D., Barnes, J. W., Sotin, C., et al. 2015, Geophysical Research Letters, 42, 3746, doi: 10.1002/2015GL063824

Niemann, H. B., Atreya, S. K., Bauer, S. J., et al. 2005, 438, 779, doi: 10.1038/nature04122

Niemann, H. B., Atreya, S. K., Demick, J. E., et al. 2010, Journal of Geophysical Research (Planets), 115, E12006, doi: 10.1029/2010JE003659

Nimmo, F., & Bills, B. 2010, Icarus, 208, 896, doi: 10.1016/j.icarus.2010.02.020

Paganelli, F., Janssen, M. A., Lopes, R. M., et al. 2008, Planetary and Space Science, 56, 100, doi: 10.1016/j.pss.2007.03.015

Palermo, R. V., Ashton, A. D., Soderblom, J. M., et al. 2024, Science Advances, 10, eadn4192, doi: 10.1126/sciadv.adn4192

Petricca, F., Genova, A., Castillo-Rogez, J. C., et al. 2023, Geophysical Research Letters, 50, e2023GL104016, doi: 10.1029/2023GL104016

Poggiali, V., Hayes, A. G., Mastrogiuseppe, M., et al. 2020, Journal of Geophysical Research: Planets, 125, e2020JE006558, doi: 10.1029/2020JE006558

Poggiali, V., Mastrogiuseppe, M., Hayes, A. G., et al. 2016, Geophysical Research Letters, 43, 7887, doi: 10.1002/2016GL069679

Poggiali, V., Brighi, G., Hayes, A. G., et al. 2024, Nature Communications, 15, 5454, doi: 10.1038/s41467-024-49837-2

Radebaugh, J., Lorenz, R., Wall, S., et al. 2011, Icarus, 211, 672, doi: 10.1016/j.icarus.2010.07.022

Raney, R. 1998, IEEE Transactions on Geoscience and Remote Sensing, 36, 1578, doi: 10.1109/36.718861

Rannou, P., Montmessin, F., Hourdin, F., & Lebonnois, S. 2006, Science, 311, 201, doi: 10.1126/science.1118424

Rodriguez, S., Le Mouélic, S., Rannou, P., et al. 2009, 459, 678, doi: 10.1038/nature08014

Rossignoli, N. L., Sisto, R. P. D., & Parisi, M. G. 2022, Astronomy & Astrophysics, 660, A127, doi: 10.1051/0004-6361/202141802

Schaller, E. L., Brown, M. E., Roe, H. G., Bouchez, A. H., & Trujillo, C. A. 2006, Icarus, 184, 517, doi: https://doi.org/10.1016/j.icarus.2006.05.025

Schinder, P. J., Flasar, F. M., Marouf, E. A., et al. 2011, 215, 460, doi: 10.1016/j.icarus.2011.07.030

Schneider, T., Graves, S. D. B., Schaller, E. L., & Brown, M. E. 2012, 481, 58, doi: 10.1038/nature10666

Schurmeier, L. R., Brouwer, G. E., Kay, J. P., et al. 2024, The Planetary Science Journal, 5, 211, doi: 10.3847/PSJ/ad7018

Schurmeier, L. R., & Dombard, A. J. 2018, Icarus, 305, 314, doi: 10.1016/j.icarus.2017.10.034

Seltzer, C., & Perron, J. T. 2023, Topographic Stress-Induced Fracturing as a Mechanism of Sediment Generation on Titan. https://agu.confex.com/agu/fm23/meetingapp.cgi/Paper/1360175

Smrekar, S., Hensley, S., Nybakken, R., et al. 2022, in 2022 IEEE Aerospace Conference (AERO) (Big Sky, MT, USA: IEEE), 1–20, doi: 10.1109/AERO53065.2022.9843269

Soderblom, L. A., Tomasko, M. G., Archinal, B. A., et al. 2007, Planetary and Space Science, 55, 2015, doi: 10.1016/j.pss.2007.04.015

Solomonidou, A., Neish, C., Coustenis, A., et al. 2020, Astronomy & Astrophysics, 641, A16, doi: 10.1051/0004-6361/202037866

Steckloff, J. K., Soderblom, J. M., Farnsworth, K. K., et al. 2020, The Planetary Science Journal, 1, 26, doi: 10.3847/PSJ/ab974e

Tan, S. P., Kargel, J. S., Jennings, D. E., et al. 2015, Icarus, 250, 64, doi: https://doi.org/10.1016/j.icarus.2014.11.029

Tokano, T. 2009, Icarus, 204, 619, doi: https://doi.org/10.1016/j.icarus.2009.07.032

—. 2013, Icarus, 223, 766, doi: https://doi.org/10.1016/j.icarus.2013.01.023

—. 2021, The Planetary Science Journal, 2, 86, doi: 10.3847/PSJ/abf049

—. 2023, Icarus, 389, 115253, doi: 10.1016/j.icarus.2022.115253

Tokano, T., & Lorenz, R. D. 2015, Journal of Geophysical Research: Planets, 120, 20, doi: https://doi.org/10.1002/2014JE004751

—. 2016, Icarus, 270, 67, doi: https://doi.org/10.1016/j.icarus.2015.08.033

Tokano, T., Lorenz, R. D., & Van Hoolst, T. 2014, Icarus, 242, 188, doi: 10.1016/j.icarus.2014.08.021

Turtle, E., Perry, J., Hayes, A., & McEwen, A. 2011, Icarus, 212, 957, doi: 10.1016/j.icarus.2011.02.005

Turtle, E. P., Perry, J. E., McEwen, A. S., et al. 2009, Geophysical Research Letters, 36, n/a, doi: 10.1029/2008GL036186

Turtle, E. P., Perry, J. E., Barbara, J. M., et al. 2018, Geophysical Research Letters, 45, 5320, doi: 10.1029/2018GL078170

US Army Corps of Engineers, . 1999. https://www.glc.org/wp-content/uploads/GLC-USACE-Living-with-the-Lakes-1999.pdf

Vu, T., Choukroun, M., Sotin, C., Muñoz-Iglesias, V., & Maynard-Casely, H. 2020, Geophysical Research Letters, 47, e2019GL086265, doi: 10.1029/2019GL086265

Wagner, N. L., James, P. B., Ermakov, A. I., & Sori, M. M. 2024, Journal of Geophysical Research: Planets, 129, e2023JE008053, doi: 10.1029/2023JE008053

Wahr, J. M., Zuber, M. T., Smith, D. E., & Lunine, J. I. 2006, Journal of Geophysical Research: Planets, 111, doi: 10.1029/2006JE002729

Wakita, S., Johnson, B. C., Soderblom, J. M., et al. 2023, The Planetary Science Journal, 4, 51, doi: 10.3847/PSJ/acbe40

Wall, S., Hayes, A., Bristow, C., et al. 2010, Geophysical Research Letters, 37, doi: 10.1029/2009GL041821

Wang, Y., & Morton, Y. J. 2022, in IGARSS 2022 - 2022 IEEE International Geoscience and Remote Sensing Symposium, 4403–4406, doi: 10.1109/IGARSS46834.2022.9884827

Wieczorek, M. 2015, in Treatise on Geophysics (Elsevier), 153–193, doi: 10.1016/B978-0-444-53802-4.00169-X

Wood, C., Stofan, E., Hayes, A., et al. 2013, in 44th Annual Lunar and Planetary Science Conference, 1764

Zebker, H., Hayes, A., Janssen, M., et al. 2014, Geophysical Research Letters, 41, 308, doi: 10.1002/2013GL058877

Čadek, O., Kalousová, K., Kvorka, J., & Sotin, C. 2021, Icarus, 364, 114466, doi: 10.1016/j.icarus.2021.114466

1421 Čadek, O., Souček, O., Běhounková, M., et al. 2019, Icarus,
1422 319, 476, doi: 10.1016/j.icarus.2018.10.003